Emerging Contaminants: Artificial Sweetener Sample Preservation and Palladium Nanoparticle Transport in Porous Media

by

Emily Marie Saurette

A thesis

presented to the University of Waterloo

in fulfillment of the

thesis requirement for the degree of

Masters of Science

in

Earth Sciences (Water)

Waterloo, Ontario, Canada, 2017

Author's Declaration

This thesis consists of material all of which I authored or co-authored: see Statement of

Contributions included in the thesis. This is a true copy of the thesis, including any required final

revisions, as accepted by my examiners.

I understand that my thesis may be made electronically available to the public.

Statement of Contributions

Chapters 2 and 3 of this thesis will be submitted as journal articles. These articles will be co-authored by myself, my supervisor – Dr. Carol Ptacek, Dr. David Blowes, Dr. Frank Gu, Dr. Mark Rivers, Stewart Linley, and Laura Groza. The majority of the contributions (data collection, figure preparation, and writing) were completed by myself. Stewart Linley synthesized the nanoparticles, and wrote paragraphs describing nanoparticle synthesis methodologies and collected nanoparticle characterization data. Dr. Mark Rivers contributed to the tomography data collection, analysis and image processing. Laura Groza contributed sections on the IC-MS/MS method for artificial sweetener analysis. Other co-authors contributed with edits and made suggestions to improve the chapters.

Abstract

Emerging contaminants are an increasing concern for regulatory bodies: artificial sweeteners and nanoparticles (NPs) included. Artificial sweeteners are found in domestic waste waters and can be used as tracers of anthropogenic impacts in groundwater and surface water. Collection procedures for aqueous samples for the analysis of artificial sweetener compounds are not delineated in standard published methods. Identifying the acceptable limits for sample collection and storage is important to provide guidelines for studies which will provide cost and time savings for industry and government agencies. Nanoparticles are used in consumer products at an increasing rate. These particles are introduced into the environment through the breakdown of these products or from accidental spills or release during manufacturing or shipping. The effects that NPs have on the environment are unknown both in terms of human and ecological health and their ultimate fate. This thesis describes two experiments on the shared topic of emerging contaminants, (1) a set of batch experiments to determine the effects of sample collection materials and storage conditions on groundwater samples for artificial sweetener analysis and, (2) column experiments to understand the transport of NPs through different porous media using a non-destructive imaging technique.

Laboratory batch experiments were conducted to determine appropriate storage methods and sampling materials to be used for groundwater samples for the analysis of artificial sweeteners. The storage methods investigated included: acidification, isolation from light, reduction of temperature, and elimination of headspace. Data were combined to evaluate the frequency distributions of concentrations at each sampling time to delineate the number of samples with analyses that fell outside of the range of 60 – 120 % of the input concentration, a range recommended to be acceptable for interpretation of data in many environmental fate

studies. Over the course of the experiment, the measured concentrations for the majority of samples fell within the acceptable range for sample preservation. The only samples with concentrations that fell outside of this range were those that were both acidified and stored at room temperature, irrespective of headspace or exposure to light. The sampling materials investigated included: three types of plastic tubing; polytetrafluoroethylene (Teflon™), styrene-ethylene-butylene co-polymer (MasterFlex™) and polypropylene (PharMed BPT™) tubing, three types of metals; aluminum, steel and stainless steel, and two types of solid plastics; polyamide (Nylon) and polyvinyl chloride. Sampling materials were submerged in simulated groundwater (SGW) to maximize contact of the sampling materials with the water samples. Artificial sweetener concentrations in aqueous samples remained constant over time in all sampling material trials, except with steel, when compared to a control test. The artificial sweetener concentration in groundwater samples in contact with steel decreased by more than 70% for each compound after 289 days (9.5 months). SEM images of the steel surfaces after 90 days (3 months) showed the presence of substantial quantities of iron oxyhydroxide precipitates and TEM images of the solution showed the presence of iron oxyhydroxide particles in suspension. These results suggest that aqueous samples for artificial sweetener analysis can be stored for up to 241 days (8 months), unless they are both acidified and stored at 25 $^{\circ}$C, and that artificial sweeteners are stable in the presence of all of the sampling materials tested with the exception of steel.

Laboratory column experiments were conducted and the transport of palladium (Pd) NPs was investigated with traditional effluent analysis and novel synchrotron x-ray computerized micro tomography (SXCMT), a non-destructive imaging technique. Five columns were packed with standard Ottawa sand, 98% Ottawa sand with 2% attapulgite clay, and, Borden sand to

understand the effect of different porous media on NP transport. The column experiments were conducted with SGW or ultrapure water (UPW). Breakthrough-curve and mass-balance data from direct analysis of Pd in effluent samples suggest that NPs are more retarded in Borden sand than in Ottawa sand. The SXCMT data used to calculate the Pd concentration in individual pores, derived from three-dimensional images of the column suggest that the Pd NP can be transported in porous media and can be quantified by the SXCMT technique.

Acknowledgements

Dedication

For everyone who I have the privilege of calling family – thank you forever.

Table of Contents

List of Tables

List of Figures

List of Abbreviations

NP	nanoparticle
GSE-CARS	GeoSoilEnviro-Center for Advanced Radiation Sources
ICP-OES	inductively-coupled plasma optical emission spectrometry
IC/MS/MS	ion chromatography followed by tandem mass spectrometry
AS	artificial sweetener
SEM	scanning electron microscopy
TEM	transmission electron microscopy
ACE	acesulfame
SAC	saccharin
SUC	sucralose
IS	internal standard
CYC	cyclamate
SXCMT	synchrotron x-ray computerized microtomography
SG(W)	simulated ground(water)
UP(W)	ultrapure (water)
3D	three dimensional
2D	two dimensional
GSV	gray scale value
REV	representative elemental volume
PV	pore volume
OD	outer diameter

ID   inner diameter

Chapter 1:

Introduction

1.1 Thesis Organization

This thesis is presented in the research paper format as two distinct studies related to separate aspects of emerging contaminants. The first chapter consists of a general introduction. Chapter 2, describes a study that systematically explores aspects related to collection, preservation and storage of water samples containing artificial sweeteners. Chapter 3 describes a study that describes a synchrotron x-ray computerized microtomography study focused on delineating mechanisms controlling transport of Pd nanoparticles (NPs) in porous media of various grain morphologies. Chapter 4 concludes this thesis with a summary of findings for both studies, their implications to the field of emerging contaminants in groundwater research, and suggestions for future directions.

1.2 Background

Emerging contaminants are a diverse group of substances that have been newly manufactured, found in the environment, or found to be harmful to the environment (Lapworth et al. 2012). These substances include many classes of chemicals: pesticides, pharmaceuticals, industrial products, personal care products (cosmetics, soaps, lotions, sunscreens, insect repellents), household products, food additives and NPs (Lapworth et al. 2012). Groundwater and surface water resources are vulnerable to inputs of these contaminants through waste-water treatment plants, agricultural and livestock-waste infiltration and runoff, hospital effluent and industrial or commercial releases. The release of emerging contaminants is poorly regulated as the effects of

these substances in the environment are not well understood. Emerging contaminants may pose a threat to humans and ecosystems at low concentrations and have not been studied as extensively as other, mainly inorganic, pollutants.

1.2.1 Artificial Sweeteners in the Environment

Artificial sweeteners have been in production since before 1970 and have been identified in environmental samples since 2009 (Buerge et al. 2009). Artificial sweeteners are used to reduce the calorie content of many beverages and food products, and are used to facilitate weaning in farm settings. Artificial sweeteners reduce calorie intake because they are not broken down by the body but still produce the sweet taste of natural sugar. This property allows artificial sweeteners to be excreted from humans and livestock untransformed and the compounds subsequently enter the environment. Artificial sweeteners fit the definition of a good tracer of anthropogenic waste water as they: (1) act conservatively in groundwater, (2) are not naturally present in the environment in high background concentrations, and (3) are inexpensive, widely used and chemically stable (Buerge et al. 2009; Davis et al. 1980). Acesulfame, sucralose, saccharin and cyclamate are found globally in consumer products.

1.2.2 Nanoparticles in the Environment

Nanoparticles are any particle, naturally occurring or manufactured that has one dimension less than 100 nm. These particles can be used for remediation of environmental contaminants by promoting degradation or sorption of contaminants. Their large surface area and unique properties give them advantages over using bulk materials and their small size allows them to be transported in porous media. Nanoparticles have been manufactured for at least 25 years (Fagan et al. 1992) and are also created naturally during weathering and other processes such as combustion (Nowack and Bucheli 2007). Nanotechnologies are developing at a rapid pace and

are incorporated into commercial and industrial products and processes to make microprocessors smaller and faster, sunscreen more effective, give fabrics antibacterial properties and to make paints that repel dirt. Nanoparticles have been successfully used in water treatment and remediation applications to promote the degradation or removal of contaminants from groundwater and waste water (Bennett et al. 2010; Su et al. 2012; Qu et al. 2013). When NPs are manufactured and used in products or remediation they have the potential to act as contaminants themselves when they pose a risk to people and the environment. Understanding their transport in groundwater will facilitate their use to allow more effective treatment of contaminants and to prevent them from being contaminants themselves.

1.3 Research Objectives: Artificial Sweetener Collection, Preservation and Storage

The research presented in this thesis is related to the understanding of emerging contaminants in groundwater. The presence of artificial sweeteners in groundwater is being used as a signature for anthropogenic wastewater impact and can be a valuable tool for groundwater-quality monitoring when samples are collected properly. The goal of the research on aqueous sample storage for the determination of artificial-sweetener concentrations in this thesis is to provide information that will benefit groundwater-monitoring efforts both in time and cost savings. Specific research questions that will be addressed in this section of the thesis are:

- How long and under which conditions can artificial sweeteners be stored before analysis?
- Which materials are appropriate for contact with artificial sweeteners during sample collection and storage?

1.4   Research Objectives: Pd NP Transport

The presence of NPs in groundwater is increasing from both intentional injections for remediation purposes and unintentionally as the release of NPs for human uses increases. The goal of the research on Pd NPs in this thesis is to further the understanding of how NPs are transported at the pore scale to improve their implementation as remediation agents and to contribute to the understanding of the risks of NPs in the environment. Specific research questions that will be addressed by this section of the thesis are:

- How can a non-destructive imaging technique (synchrotron x-ray computerized micro-tomography; SXCMT) be used to understand Pd NP transport under various conditions?

- Do the properties of pore spaces influence Pd NP transport and can this influence be evaluated with SXCMT?

Chapter 2:

Storage and Preservation of Artificial Sweeteners in Groundwater

Samples

2.1 Summary

Compound specific standardized sampling and storage methods are currently not available for artificial sweeteners. The goal of this study is to understand: (1) the appropriate length of time for storage of samples containing these compounds, (2) under which conditions they remain stable, and (3) which sampling materials are appropriate for sample collection. This knowledge will improve the use of artificial sweeteners in environmental studies. Batch studies were used to analyze the stability of acesulfame (ACE), sucralose (SUC), saccharin (SAC), and cyclamate (CYC) in simulated groundwater (SGW) with various sample collection materials and under varying preservation and storage conditions. The storage conditions that were evaluated were acidification, headspace, exposure to light and refrigeration, and, the sampling materials evaluated were steel, stainless steel, aluminum, polyvinyl-chloride, polyamide (Nylon), polypropylene (PharMed BPT™) tubing, styrene-ethylene-butylene co-polymer (MasterFlex™) tubing and polytetrafluoroethylene (Teflon™) tubing. All artificial sweetener compounds evaluated were observed to be stable in storage at 4$°$C for at least 241 days (8 months). Concentrations of artificial sweeteners were consistently within 0.6 – 1.2 of the original concentration with the exception of ACE and SAC that were substantially lower under acidified conditions at 25$°$C after 241 days. Artificial sweetener concentrations remained nearly constant while in contact with all of the sampling materials, with the exception of steel. SEM and TEM images showed that oxidation of steel had occurred and all compounds were extensively removed from aqueous solution at 289 days. These results suggest that optimal results are obtained for artificial sweetener analyses conducted within 14 days of sample collection, however under certain conditions longer storage times may be acceptable. The results also

suggest that concentrations of artificial sweeteners in SGW were not affected by extended contact with typical well casing, sampling and storage materials, with the exception of steel.

2.2 Introduction

The presence of artificial sweeteners in environmental water samples is an important indicator of water quality, including the impact of wastewater on surface and groundwater bodies. Artificial sweeteners are introduced into the environment by domestic wastewater discharge and are persistent long distances from their source (Liu et al. 2014). The use of artificial sweeteners as tracers is becoming widely applied because of the conservative behavior and widespread occurrence of these compounds in the environment (Liu et al. 2014).

The proper handling and preservation of samples collected during laboratory and field studies is extremely important to obtain representative analyses to determine the fate of emerging contaminants in the environment. Studies that compare the collection, preservation and storage techniques for analysis of pesticides, chlorinated hydrocarbons, pharmaceutical compounds, personal care products, steroids, hormones, and other organic pollutants and products in water samples are available (Mompelat et al. 2013; U.S. EPA 2010; Bartram et al. 1996; Reynolds et al. 1990), however similar studies are not available for artificial sweeteners. Information on collection, preservation and storage of water samples provided by regulatory agencies consists of three main sources: a study produced by the United States Environmental Protection Agency (EPA) to modify methods 1694 and 1698 (U.S. EPA 2010), Water Quality Management Sampling Guide produced by the World Health Organization (Bartram et al. 1996) and the Water Quality Sampling Standard produced by the International Organization for Standardization (ISO, 2012). This information provides appropriate methods and standards for the collection of water samples for the analysis of volatile and sensitive organic compounds.

The sampling and storage protocols recommended by the above regulatory agencies are not specific to artificial sweeteners but are generalized for organic compounds: the recommendations are often highly restrictive and/or inappropriate for artificial sweeteners which are resistant to degradation. The Water Quality Management Sampling Guide recommends collecting samples in amber glass bottles, and outlines preservation methods (including cooling and acidification),holding times for various organic compounds, and for all organic compounds to be extracted on site or immediately upon return to the laboratory (Bartram et al. 1996). The U.S. EPA conducted a study to update their method for preserving organic compounds which recommends using either amber high density polyethylene (HDPE) or amber glass containers, storage below 6°C in the dark, extraction of samples within 7 days, and analysis of the extracts within 30 days (U.S. EPA 2010). The Water Quality Sampling Standard produced by ISO was not freely accessible for consultation and therefore was not evaluated here. A gap remains related to the sampling, preservation and storage of water samples for artificial sweeteners which are generally more resistant to degradation than other organic compounds.

Studies that addressed methodologies for the collection and storage of water samples containing artificial sweeteners were conducted to validate the methods of storage specific to their studies (e.g., Van Stempvoort et al. 2011; Berset and Ochsenbein 2012). These studies found that filtered environmental samples for ACE and SUC analysis were unaffected by refrigeration or freezing, whereas SAC and CYC concentrations were stable during freezing but were degraded at 4°C (Van Stempvoort et al. 2011). These studies suggested a holding time of one week, however, samples in the study were stored for up to one year before analysis (Van Stempvoort et al. 2011). Berset and Ochsenbein (2012) determined that aspartame in spiked

groundwater did not degrade when stored at 4°C with an adjusted pH of 4.3 for 8 days, but did degrade when stored at 25°C or at 4°C at neutral pH.

In this study, the effects of sampling materials, preservation methods and storage times on the stability of artificial sweetener compounds in SGW were evaluated. The artificial sweeteners included in this study were ACE, SUC, SAC and CYC. The stability of the target compounds in aqueous samples is defined as a compound that retains 60 – 120% of its original concentration following Fedorova et al. (2014).

2.3   Materials and Methods

Batch experiments were conducted to evaluate the effect of long term contact with sampling materials, and to evaluate the stability of artificial sweeteners under various standard environmental laboratory storage conditions for up to 241 days (8 months).

2.3.1   Reagents and Solutions

Artificial sweetener compounds, ACE, CYC, SUC, and SAC were obtained from Sigma-Aldrich (Oakville, Canada). The structure and relevant properties of the artificial sweeteners are provided in Table 2.1. The isotope-labeled standards, acesulfame-d4, sucralose-d6, saccharin-^{13}C6 and cyclamic acid-d11, were obtained from Toronto Research Chemicals Inc. (Toronto, Canada). HPLC-grade acetonitrile, sodium acetate and acetic acid were purchased from VWR (Mississauga, Canada). Ultrapure water (UPW, Type 1) was generated by a MilliQ A10 water system (18.2 MΩ cm @ 25°C). Simulated groundwater was prepared by adding reagent grade $CaCO_3$ (3.6 mg L^{-1}) to UPW and bubbled with CO_2 gas followed by equilibration with atmospheric CO_2. Concentrated stock solutions of each artificial sweetener were made by dissolving the solid analytes in UPW to obtain a concentration of 1 g L^{-1}. A mixed stock solution containing all four artificial sweetener compounds was prepared by serial dilution in UPW to a

concentration of 10 mg L^{-1}. The SGW was spiked with the mixed stock solution to obtain an initial concentration of 100 μg L^{-1} of all four artificial sweeteners for use as an input solution in the experiments.

2.3.2 Batch Test to Evaluate Contact with Sampling Materials

A range of materials typically used during environmental sampling were used in this experiment, and included: polytetrafluoroethylene (Teflon™) tubing (Tubefit, Toronto, Canada), polypropylene (PharMed BPT™) tubing (Cole-Parmer, Montreal, Canada), styrene-ethylene-butylene co-polymer (MasterFlex C-Flex™) tubing (Cole-Parmer, Montreal, Canada), polyamide (Nylon) (Sabic Polymershapes, Brampton, Canada), polyvinyl-chloride (Sabic Polymershapes, Brampton, Canada), aluminum (Canada Steel, Cambridge, Canada), steel (Kitchener Steel, Kitchener, Canada) and stainless steel (Kitchener Steel). The materials were cut to size, measured, washed and placed in 250 mL amber glass bottles (VWR, Mississauga, Canada) with polytetrafluoroethylene (Teflon™) caps (Table 2.2). The bottles were then filled with 200 mL of the 100 μg L^{-1} artificial sweetener input solution. Sacrificial sampling of one bottle occurred at each time point in the experiment. Samples were collected using disposable Nalgene™ syringes (Thermofisher Scientific, MA, USA), and filtered with 0.45 μm Nalgene™ membranes (Thermofisher Scientific, MA, USA). Solid steel pieces were collected for scanning electron microscopy analysis (SEM) at the 42-day time point, allowed to air dry and were stored in an empty glass bottle until analysis. Unfiltered samples of the SGW in contact with steel for 78 days were collected with no headspace and stored in a clear glass bottle until analysis by transmission electron microscopy (TEM).

2.3.3 Batch Test to Evaluate Storage Techniques

A range of storage techniques were evaluated in this experiment. Simulated groundwater samples spiked with artificial sweeteners were stored under different combinations of conditions, including: acidification, refrigeration, isolation from light and reduction of headspace. Samples were also stored in two types of 15 mL containers, polypropylene bottles (VWR, Mississauga, Canada) and clear glass vials (VWR, Missisauga, Canada). Acid-preserved samples were acidified with reagent grade 9N H_2SO_4 to a pH of below 2. Samples that were refrigerated were kept below 4 °C and were in an environment where light was limited. Light reduction was achieved by taking precautions to avoid light contacting the sample. The total elimination of light was not attempted in samples stored under refrigeration to emulate typical storage conditions with periodic exposure to light, therefore samples are not considered to be stored in a light-free environment. Light is defined as any visible radiation, either coming from the sun or a source such as lamps. Samples that were kept at 25°C were protected from light by storage in a cardboard box wrapped in aluminum foil or exposed to light by storage in a clear plastic container. Headspace was varied by either filling the sample bottle to allow no headspace or by filling with 10 mL of sample to allow approximately one third of headspace. Sacrificial sampling of one bottle of each combination of storage techniques, occurred at each time point in the experiment. Samples were transferred to disposable Nalgene™ syringes and filtered with 0.45 μm Nalgene™ membranes prior to storage for analysis.

2.3.4 Artificial Sweetener Analysis

Artificial sweetener compounds were analyzed, using direct injection ion chromatography (Dionex ICS-5000 system, Sunnyvale, CA, USA) followed by electrospray tandem mass spectrometry (Agilent 6460 QQQ, Missisauga, Canada) modified from the method described by

Van Stempvoort et al. (2011). The Dionex ICS-5000 system contained an analytical column (Dionex RFIC™ IonPac® A520, 2 x 250 mm), and a guard column (Dionex IonPac™ AG20 RFIC™, 2 x 50 mm). The potassium hydroxide eluent gradient was used according to the method described by Van Stempvoort et al. (2011). The retention times of the four artificial sweeteners, ACE, SUC, SAC, and CYC, were determined to be: 7.1, 2.9, 9.3, and 3.7 minutes respectively. For each compound the Agilent 6460 Triple Quad MS was operated in electrospray ionization negative mode and multiple-reaction monitoring (MRM) mode. The source parameters were optimized to and set to: sheath gas flow 11 L min^{-1}, sheath gas temperature 350 ℃, drying gas flow 10 L min^{-1}, drying gas temperature 225 ℃, nebulizer pressure 45 psi, capillary voltage 3600 V, and fragmentor voltage 100 V, which provided the best signal for the analytes and internal standards. The multiple reaction monitoring (MRM) transitions that were selected for quantitative analysis for analytes and internal standards (IS) were: SUC (IS) m/z 403.0 – 350.0, SUC (analyte) m/z 397.0 – 350.0 and m/z 395.2 – 350.0, SAC (IS) m/z 187.9 – 106.0, SAC (analyte) m/z 181.8 – 105.8, CYC (analyte) m/z 178.2 – 80.0, ACE (IS) m/z 166.1-86.1, ACE (analyte) m/z 162.1 – 81.8 and m/z 162.1 – 78.0.

For instrument calibration, standard stock solutions of 1 g L^{-1} were prepared by dissolving each compound in water. Standard solutions containing all four analytes were prepared by serial dilution in water. A 9-point standard curve was created in the range 0.1 - 200 µg L^{-1} for each of the artificial sweeteners. Prior to analysis, samples were filtered with 0.22 µm PVDF (polyvinylidene difluoride) membranes (Chromatographic Specialties Inc., Brockville, ON, CAN) and disposable Nalgene™ syringes. Then 1 mL aliquots of aqueous sample were spiked with 10 µL of internal standard to a final concentration of 50 µg L^{-1} for ACE, SAC and CYC, and, 200 µg L^{-1} for SUC. The method detection limits (MDLs) were determined by

analyzing seven samples at a concentration five times lower than the lowest standard concentration and multiplying the standard deviation of the measured concentrations by the Student's t value at $n-1$ degrees of freedom. The MDLs calculated were: 0.12 μg L^{-1} for ACE, 0.57 μg L^{-1} for SAC, 0.31 μg L^{-1} for CYC, and 0.28 μg L^{-1} for SUC.

Duplicate and continuous calibration-verification samples were run after every 10 unknown samples. All laboratory blanks had artificial-sweetener concentrations below the MDLs. Absolute analyte and internal standard recoveries for calibration samples were between 86 and 115%. Relative internal standard recoveries for unknown samples were 72 to 111%. Recoveries of duplicate, repeated, or spiked samples were 89 to 134%.

2.3.5   Electron Microscopy Analysis

SEM images of solid steel were collected at the University of New Brunswick with a JEOL 6400 SEM using secondary electron imaging with Geller dPict digital image acquisition software. TEM images of suspended nano-particulate matter were collected at the University of New Brunswick with a JEOL 2011 STEM using brightfield in conventional mode used for elemental recognition and phase identification as well as quantitative compositional analysis.

2.4   Results and Discussion

2.4.1 Impact of Storage Conditions on Artificial Sweetener Stability

A variety of different combinations of storage conditions were distributed over 24 samples at each time point in the experiment. These samples represent all of the possible combinations of chosen storage conditions. The combinations include: refrigeration, acidification, reduction of light and reduction of headspace in either clear glass or polypropylene bottles and were evaluated over 241 days to determine the overall stability of aqueous artificial sweetener compounds (Fig. 2.1). The relative concentrations of artificial sweeteners present in

the aqueous samples were determined by dividing the measured concentration in the sample by the mean measured concentration of the initial input solution (n=3). The concentration data is grouped into 24, 5% bins, from 0 – 120%, to illustrate the frequency that aqueous concentrations of the artificial sweeteners occurred relative to the original input solution (Fig. 2.2). Artificial sweetener concentrations were observed to fall within the range of 15 – 120% of the initial concentration over the duration of sample storage for all samples.

The compounds ACE, CYC and SAC have low pK_a (1.6 – 2.0) and log K_{ow} (-2.63 – 0.91) values (Table 2.1). At ambient pH these compounds will deprotonate and be present as anions in solution. Compounds with low log K_{ow} values are hydrophilic and soluble in water. Sucralose is a base (pK_a 12.5), and remains protonated at ambient pH, and is soluble in water (log K_{ow} -1.00) because the alcohol functional groups allow hydrogen bonding to occur with water (Table 2.1).

Analyses of the SGW samples under different storage conditions indicate that aqueous artificial sweetener concentrations under most storage conditions were relatively constant over the 241 day (8 month) study duration (Fig. 2.2). Aqueous samples, independent of storage method, analyzed after three days of storage had artificial sweetener concentrations of between 75% and 105% of the original input concentration for all four compounds, ACE, SUC, SAC, and, CYC. After 14 days, 32 days and 241 days the relative concentration ranges were 75 - 110%, 80 - 115% and, 15 - 120% respectively (Fig. 2.2), showing an increasing variability of the aqueous artificial-sweetener concentrations over time. At 241 days the range of relative concentrations had the broadest distribution indicating that the compounds became increasingly unstable over time.

The stability of each individual compound, and the precision and accuracy of the method of analysis, will affect the relative concentration distribution reported for each artificial

14

sweetener. After 241 days of storage, the concentration of cyclamate in the aqueous samples was the most consistent with most samples having a relative cyclamate concentration between 75 – 115 % at all time points. The relative stability of the compounds over time was CYC>SUC>ACE>SAC determined by the range of relative concentrations measured (Fig. 2.2). The widest concentration distribution at 3 days was obtained for aqueous concentrations of CYC, but over the course of the experiment the concentration distribution was more consistent than for the other compounds. The concentrations of SUC in aqueous samples stayed within 90 – 110% of the initial concentration up to 32 days, and at 241 days had a wider distribution indicative of instability. The concentrations of ACE and SAC in aqueous samples had similar distributions to CYC and SUC, but at 32 days developed a bimodal distribution and at 241 days had separated into two distinct populations. After 241 days of storage under various conditions, the measured artificial sweetener concentrations had the widest distribution than at any other time point. However, most were still considered stable with their concentrations falling between 60 and 120% of the input concentration, following the definition of stability by Fedorova et al. (2014) (Fig. 2.2). The preservation method of the samples can affect concentration over time and may explain the differences in relative stability over time.

Storage and sample preservation methods can lead to increased degradation of some compounds. The only samples that were not stable after 10 days were samples containing ACE and SAC that were acidified and stored at 25°C, irrespective of headspace or exposure to light (Fig. 2.1). This combination of preservation techniques was the only combination that promoted the removal of ACE and SAC after extended storage. Samples that were acidified and kept at 4°C, and samples that were kept at 25°C but were not acidified, had stable aqueous ACE and SAC concentrations. These compounds have structural similarities as both contain secondary

15

sulfonamide functional groups where the N atom is bound to a carbonyl group (Table 2.1). Acid catalyzed hydrolysis can potentially transform ACE and SAC as has been shown for atrazine, a common herbicide (Prosen and Zupančič-Kralj 2005); however, monitoring of reaction products is required to confirm this mechanism. All other storage combinations, for all four compounds, did not result in samples with aqueous artificial sweetener concentrations outside of the acceptable range of stability.

Over time, artificial sweetener samples will degrade slowly. These effects are mitigated by analyzing samples before these reactions can proceed to an extent when the concentration of the analyte that is being measured is outside of 60 – 120% of the original concentration (Fedorova et al. 2014). Generally, for pharmaceuticals, which are often analyzed with artificial sweeteners, an acceptable loss of compound is up to 40% of the original concentration (Fedorova et al. 2014). The stability, however, is difficult to determine if the samples are not analyzed twice, once immediately after collection and once at a later date for direct comparison.

The proper storage of aqueous samples for artificial sweetener analysis is important for their use as tracers or in studies to determine their environmental fate. Many preservation techniques attempt to prevent or slow the natural degradation of compounds of interest. Storing samples at 4ºC can slow reactions and bacterial degradation (U.S. EPA 2010). Acidification of samples also attempts to preserve the compound of interest by minimizing complexation reactions and growth of bacteria (U.S. EPA 2010). These conditions can therefore render the bacteria unable to catalyze degradation reactions. The only combination of preservation techniques that resulted in unstable ACE and SAC concentrations were acidification at 25ºC. Heat combined with low pH may encourage decomposition reactions (Sang et al. 2014). With increased time of storage, a greater spread in concentration frequency distributions was observed

for ACE, SUC and SAC indicating these compounds reacted differently under the different combinations of storage and preservation conditions (Fig. 2.2).

Artificial sweeteners are persistent in the environment and samples containing these compounds can be stored for extended periods of time in the laboratory. Optimum results, however, are obtained when samples are analyzed immediately after collection. When immediate analysis is not possible artificial sweetener samples may remain stable for 241 days (8 months) with proper storage. Ideal storage conditions include holding samples at 4^oC without acidification, but do not significantly depend on bottle material (plastic or glass) or headspace. Environmental samples should be filtered to remove particulate matter that may promote sorption of artificial sweeteners from the sample before storage. The results here relate to the analysis of artificial sweeteners using an IC/MS/MS technique. Artificial sweeteners can be quantified using many different techniques and it is important to ensure that the preservation technique applied to the sample is compatible with the analysis method employed. For example, chlorine interferes with IC/MS/MS analysis of cyclamate as cyclamate elutes at a similar time as chlorine (Van Stempvoort et al. 2011).

2.4.2 Impact of Sampling Materials on Artificial Sweetener Stability

Three major classes of materials are commonly used for collection of groundwater samples: plastic tubing, bulk plastics and bulk metals. These materials are used in wells, pumps and collection apparatuses. Artificial sweeteners were placed in contact with eight different materials for 289 days (9.5 months) to simulate long-term contact of groundwater samples with groundwater sampling materials that may occur with improper techniques, such as not purging a well before sample collection. The concentration of each artificial sweetener was measured in the SGW in contact with the materials and the absolute concentrations were plotted over time. A

total of seven time points were selected to observe the relationship between the concentration of artificial sweeteners in the simulated groundwater as a function of time. Each compound responded similarly, however are plotted separately to highlight the individual materials tested (Fig. 2.3, ACE; Fig. 2.4, CYC; Fig. 2.5, SAC; Fig. 2.6, SUC).

Most aqueous samples in long term contact with sampling materials had relatively constant aqueous concentrations of artificial sweeteners. Artificial sweetener concentrations in groundwater in contact with plastic tubing, bulk plastics, aluminum and stainless steel remained above 80% of the original input concentration for the entire duration of the experiment, 289 days (9.5 months: Figs. 2.3 – 2.6). Therefore, there was likely no degradation or sorption of artificial sweeteners relative to the control by any plastic tubing, bulk plastics, aluminum or stainless steel used in this experiment. Steel was an exception and over time extensive decreases in artificial sweetener concentration in SGW in contact with steel were observed. Over 289 days the aqueous concentrations of all artificial sweeteners decreased in the SGW that contained steel (Figs. 2.3 – 2.6). The aqueous concentrations of ACE and CYC in samples containing steel were less than 1% of the original concentration after 289 days (Fig. 2.3, 2.4). The aqueous concentrations of SUC and SAC were less than 30% of the original concentration after 289 days (Fig. 2.5, 2.6). The removal of each compound by steel follows an exponential regression fit represented by the following equation:

$$C(t) = a + be^{-\lambda t}$$

where *C* represents the concentration in aqueous solution, *a* represents the concentration remaining in aqueous solution at $t = \infty$, *b* represents the initial concentration of the removable fraction of the compound ($\mu g\ L^{-1}$), $a + b$ represents the initial concentration, and λ represents the removal constant (days^{-1}). The removal constant decreases in order of ACE>CYC>SAC>SUC

(Table 2.3). The removal rate decreases as the concentration of artificial sweeteners decreases in the aqueous solution.

Solid steel samples that likely promoted the removal of artificial sweetener compounds from the SGW samples had developed a rust coloured coating on the surface, the aqueous solution had also developed a similar colour suggesting that particles were released into suspension in the aqueous solution. The SGW that was sampled from the steel test bottle was orange in color and the solid steel had a mottled bright orange and red coating. Samples of the SGW from the steel test bottle were imaged with a TEM and the particles that were observed in the solution consisted of various sized aggregates of iron oxyhydroxide sheets or flakes greater than 500 nm in diameter (Fig. 2.7). SEM images showed the two morphologies of iron oxyhydroxide, rounded, and rosette or intersecting sheets, that formed on the surfaces of the solid steel (Fig. 2.8). The rate of iron oxyhydroxide formation increased with time as the removal of artificial sweeteners from the aqueous solution continued. Zero valent iron (ZVI) has been used to catalyze the degradation of organic compounds such as chlorinated hydrocarbons (Lien and Zhang 2001; Su et al. 2012; Dominguez et al. 2016) and has also been shown to remove organic contaminants from aqueous solutions through adsorption and inclusion in precipitates (Tomizawa et al. 2016).

The formation of iron oxyhydroxide particles and their release into SGW from the steel surface (Figs. 2.7, 2.8) suggest that there is potential for regeneration of the steel to continue catalysis of artificial sweeteners. As the steel oxidizes it produces iron oxyhydroxides which have a highly positive surface charge. These particles are not strongly bonded to the steel surface. The rate of oxidation of steel is also accelerated by carbonate ions produced from the dissolution of calcium carbonate (Garverick, 1994). Organic compounds that can have negatively

19

charged functional groups, like humic acid (a main component of dissolved organic matter) and similarly ACE, CYC, SAC and SUC (Table 2.1), are favorably sorbed to positive iron oxyhydroxide surfaces (Tessier et al. 1996). The iron oxyhydroxide particles likely attract artificial sweeteners to adsorb on to their surfaces, remove them from aqueous solution, and potentially promote their degradation(O'Carroll et al. 2013).

2.5 Conclusions

Samples should be analyzed as rapidly as possible to obtain optimal results. Samples, with SGW matrices with no natural dissolved organic carbon/matter (DOC/M), containing the artificial sweeteners SUC, SAC, CYC and ACE in SGW may be stored in conditions at or below 4°C for at least 241 days (8 months). Samples for determination of ACE and SAC concentrations should not be acidified if samples are stored at 25°C.

When collecting samples for artificial sweetener analysis, the concentrations in samples in contact with polytetrafluoroethylene (Teflon™) tubing, polypropylene (PharMed BPT™) tubing, styrene-ethylene-butylene co-polymer (Masterflex C-Flex™) tubing, polyamide (Nylon), polyvinyl chloride, aluminum and stainless steel were not altered by sorption or degradation, suggesting that these materials may be appropriate for use. Water samples should not be in contact with steel for an extended period of time to minimize degradation of artificial sweeteners.

Cost savings can be achieved by understanding the preservation of artificial sweetener compounds in water samples and creating a guideline for acceptable collection methods and storage times. Understanding sample collection and storage procedures allows researchers to have confidence in observed artificial sweetener concentrations. Reliable results are paramount

to the interpretation of studies that utilize artificial sweeteners as tracers or indications of

anthropogenic influence on water systems.
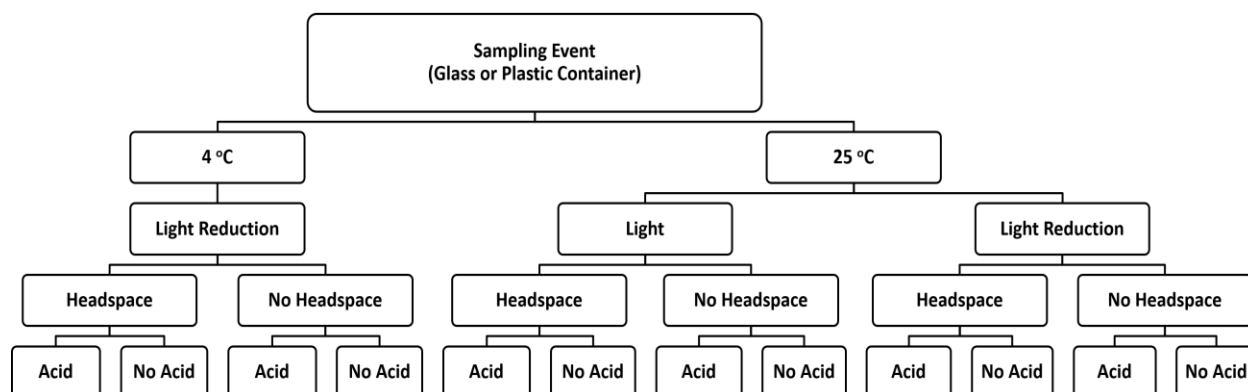
Figure 2.1. Flow chart of how preservation methods were combined in each sample. A total of 24 samples were collected at each sampling time as this flow chart represents the preservation methods that were tested for each type of bottle, plastic or glass.
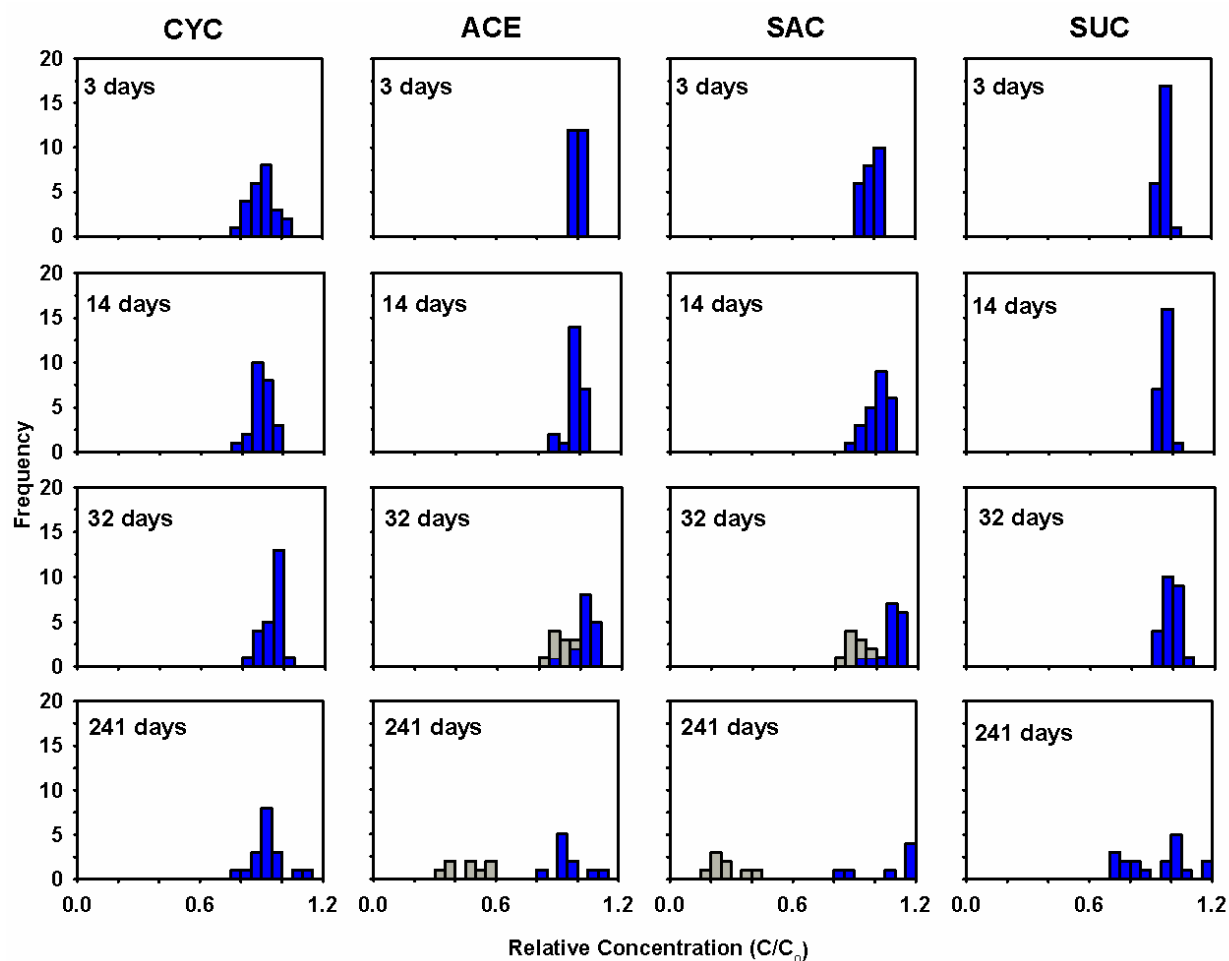
Figure 2.2. Concentration distributions for artificial sweeteners at sampling times of 3, 14, 32 and 241 days. All preservation methods are grouped together. The grey bars shown in the 32 and 241 day plots for ACE and SAC represent samples that were acidified and stored at 25°C irrespective of headspace or exposure to light. The range of relative concentrations that can be considered stable is 0.6 - 1.2. Samples acidified and kept at 25 °C were the only samples to have measured concentrations below 60% of the input concentration.

ACE
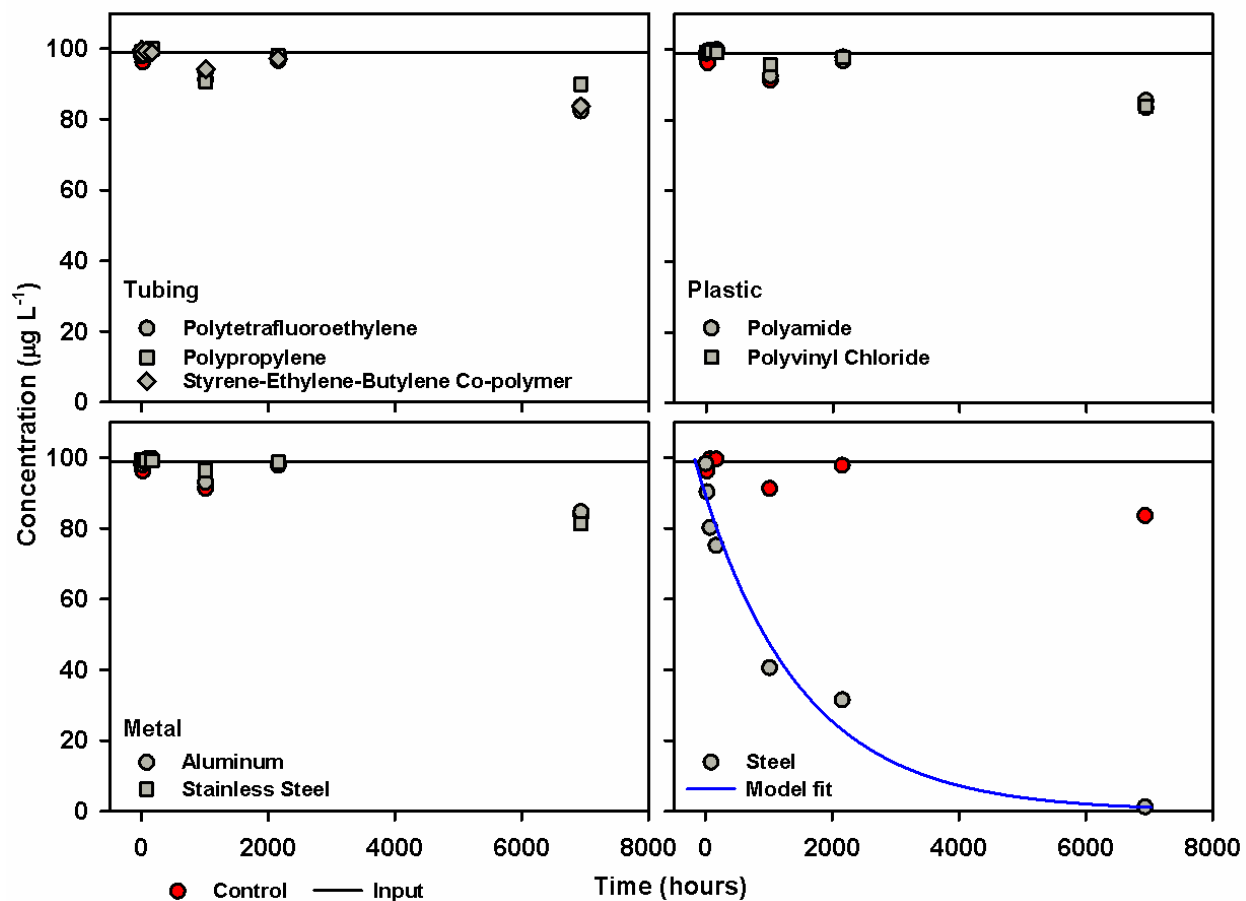
Figure 2.3. Concentrations of ACE as a function of time when exposed to various sampling materials. Sampling materials are grouped by type: tubing (top left), plastics (top right), metals (bottom left) and steel (bottom right).

24
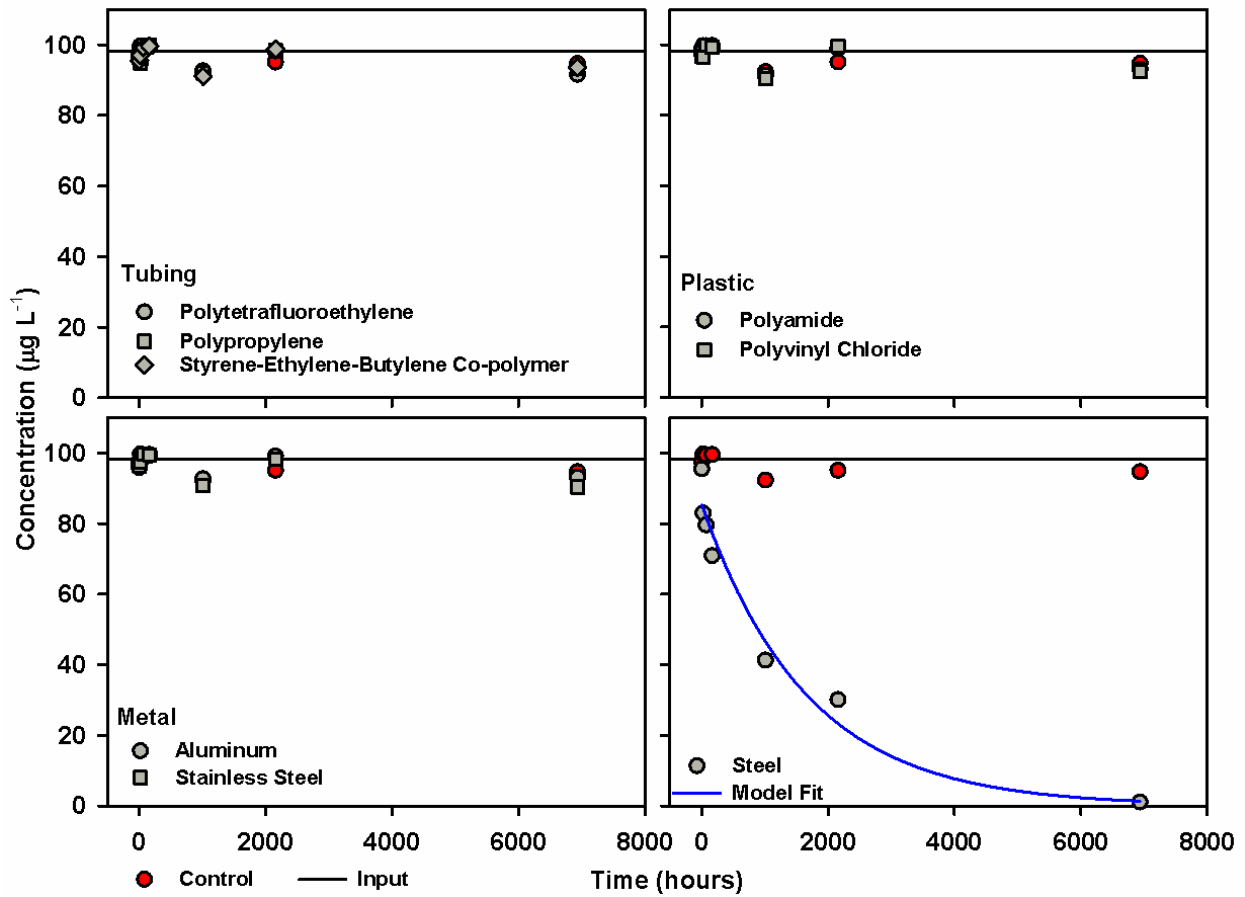
Figure 2.4. Concentrations of CYC as a function of time when exposed to various sampling materials. Sampling materials are grouped by type: tubing (top left), plastics (top right), metals (bottom left) and steel (bottom right).
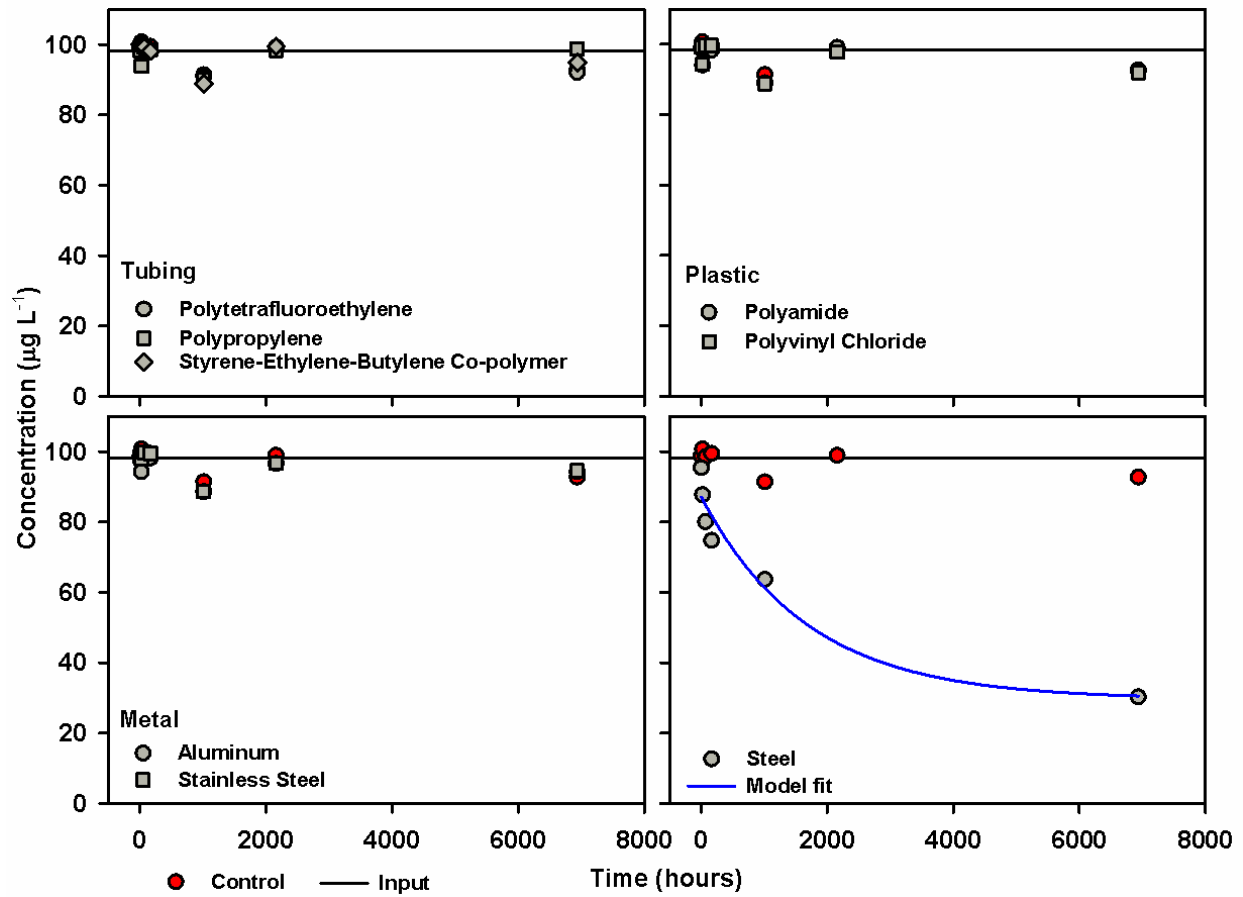
Figure 2.5. Concentrations of SAC as a function of time when exposed to various sampling materials. Sampling materials are grouped by type: tubing (top left), plastics (top right), metals (bottom left) and steel (bottom right).
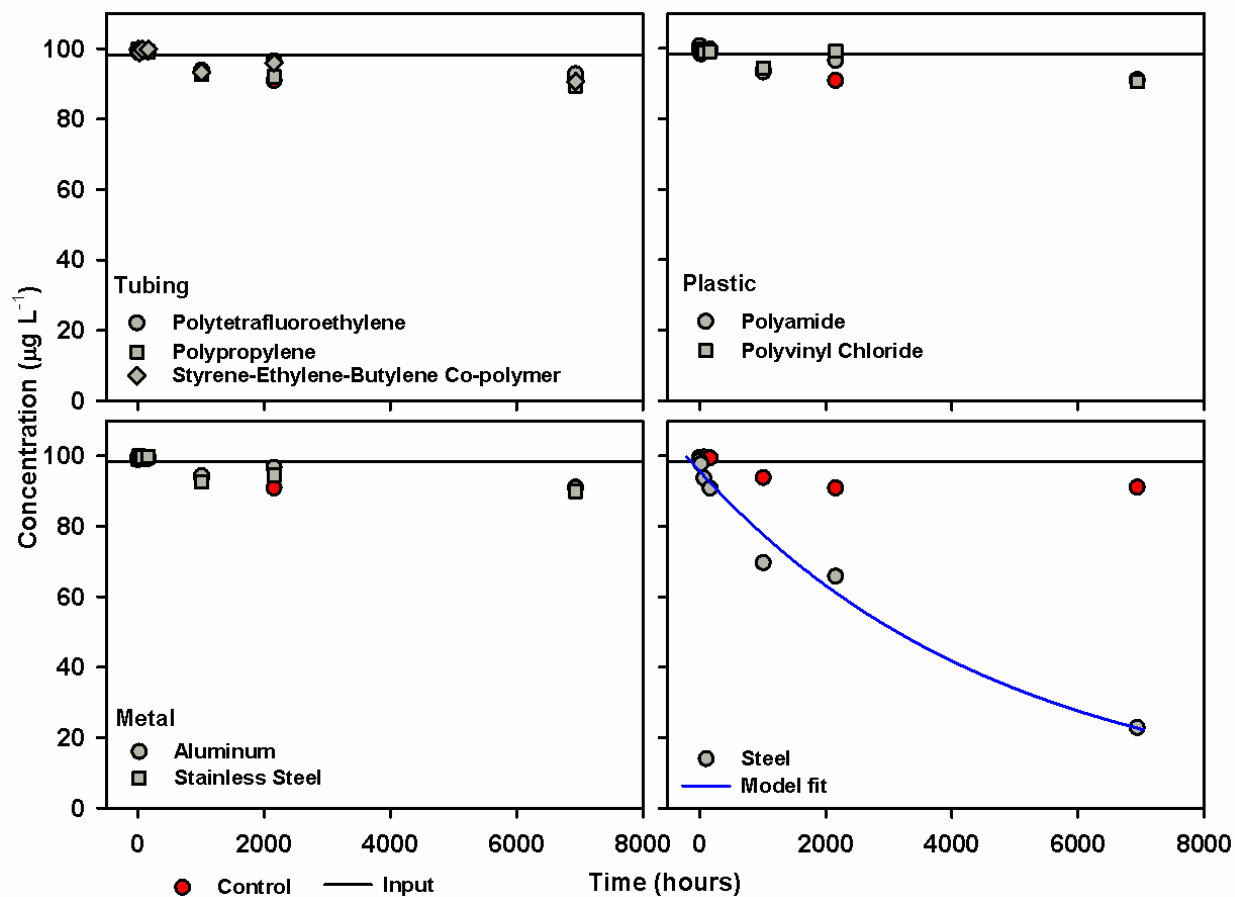
Figure 2.6. Concentrations of SUC as a function of time when exposed to various sampling materials. Sampling materials are grouped by type: tubing (top left), plastics (top right), metals (bottom left) and steel (bottom right).
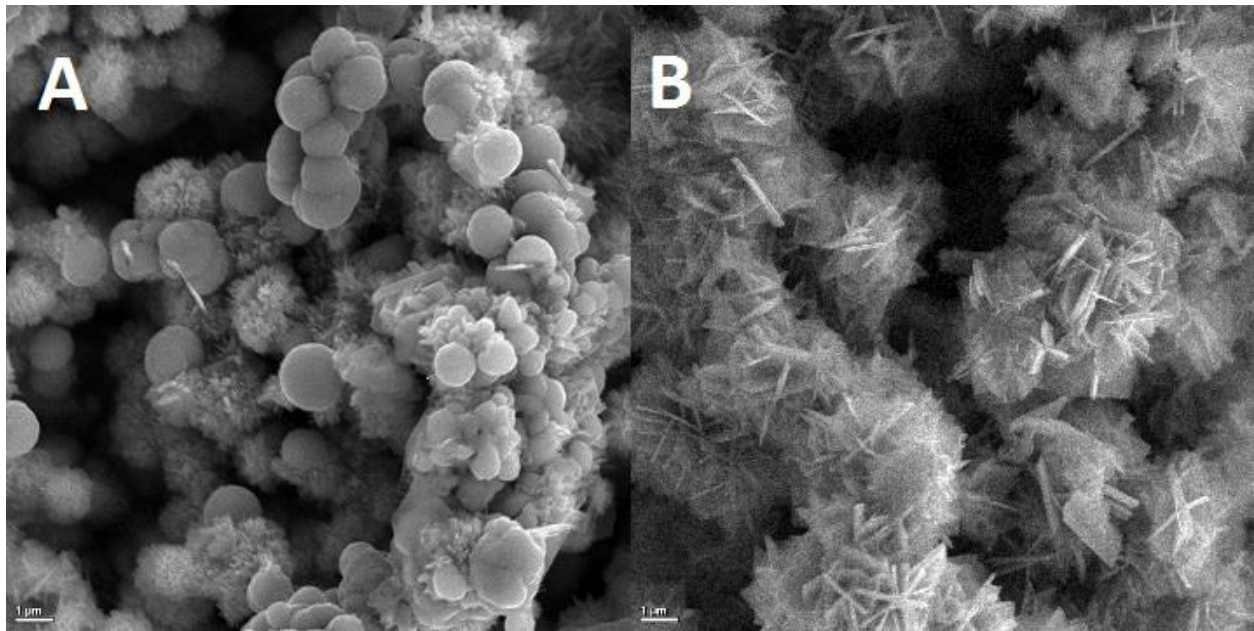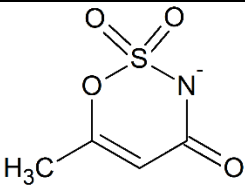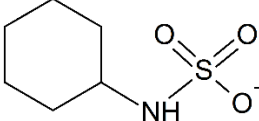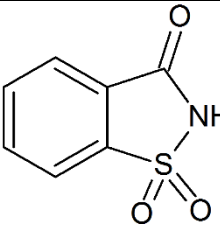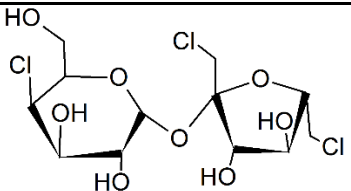
Figure 2.7. (A) An SEM image of the surface of steel after being submerged in simulated groundwater spiked with artificial sweeteners for 90 days (3 months): very little rust was present at the beginning of the experiment. **(B)** An SEM image of the surface of steel after being submerged in simulated groundwater spiked with artificial sweeteners for 90 days (3 months). A different morphology of rust is seen in this image
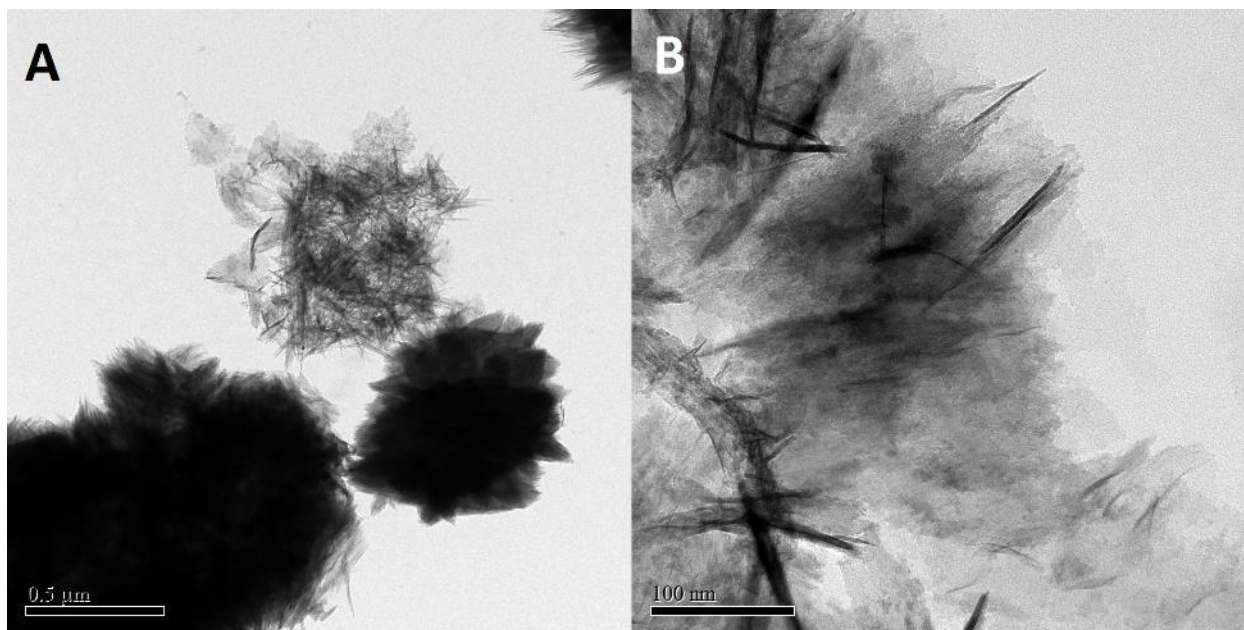
Figure 2.8. TEM images of iron oxy-hydroxide particles in simulated groundwater spiked with artificial sweeteners after being in contact with steel for 90 days (3 months); no particulate matter was present in the simulated groundwater at the beginning of the experiment. **(A)** Particles present in the simulated groundwater vary in size an density and are composed of sheets of iron oxy-hydroxide. **(B)** Intersecting sheets that compose iron oxy-hydroxide do not have a crystalline structure.

Table 2.1 Artificial sweetener compounds used in batch experiments and their structure, pK_a and log K_{ow} values.

Compound	Structure	pKₐ	Log Kₒw
Acesulfame		2.0	-1.33
Cyclamate		2.0	0.91
Saccharin		1.6	-2.63
Sucralose		12.5	-1.00

Table 2.2 Material type and composition used in the batch experiments and their mass and surface area. Range indicates the differences among sample times.

Material	Composition	Mass (g)	Surface Area (cm^2)
Tubing	polytetrafluoroethylene (Teflon™)	1.22 – 1.36	28.1 – 31.6
	polypropylene (PharMed BPT™)	0.90 – 0.94	21.2 – 22.7
	styrene-ethylene-butylene co-polymer (MasterFlex™)	3.04 – 3.22	44.8 – 48.7
Plastic	PVC	3.36 – 7.08	13.1 – 18.1
	Polyamide (Nylon)	4.33 – 5.09	17.3 – 19.6
Metal	Aluminum	6.44 – 21.22	12.6 – 24.4
	Steel	17.52 – 20.01	13.0 – 14.4
	Stainless Steel	7.39 – 12.11	8.59 – 10.9

Table 2.3 Values for variables in exponential regression fits to rate data from batch experiments with artificial sweetener compounds in contact with steel. Exponential regression fits follow the equation $C(t) = a + be^{-\lambda t}$.

Compound	a (µg L^{-1})	b (µg L^{-1})	λ (days^{-1})
Acesulfame	0	89.6	0.006
Cyclamate	0	85.6	0.0006
Saccharin	29.6	57.7	0.0006
Sucralose	5.0	91.0	0.0002

Chapter 3:

Transport of Pd Nanoparticles in Porous Media of Varying Grain Size

with Synchrotron X-Ray Computerized Tomography

3.1 Summary

Understanding the transport of nanoparticles (NPs) in porous media is a fundamental aspect of assessing the fate of NPs in the environment, both as emerging contaminants and as remediation agents. The properties of the porous media, aqueous solution and NPs affect the to transport of NPs in subsurface environments. In this study, Pd-NP transport through porous media was evaluated in column experiments containing Ottawa sand, Ottawa sand and clay, and Borden sand, together with two aqueous solutions, ultrapure water (UPW) and simulated groundwater (SGW) using traditional effluent breakthrough curves (BTC) and nondestructive synchrotron x-ray computed microtomography (SXCMT) imaging analyses. Inverse modelling using the computer code, CXTFIT STANMOD, was used to inversely determine dispersion coefficients (D) and retardation factors (R) from the BTC data for each column. Nanoparticle transport was more retarded in porous media with smaller grain size, or, higher grain surface area, and greater mineralogical diversity (Borden sand) compared to uniform clean sand (Ottawa sand). The retardation of NPs also increased with simulated groundwater as the carrier solution. Five three-dimensional images were collected for each column using SXCMT difference imaging which provided estimates of aqueous Pd NP concentrations in thin slice sections and in individual pore spaces. SXCMT difference imaging was used to evaluate the concentration of NP within porous media at the pore scale to facilitate understanding of NP transport processes and show that the Pd concentration distributions vary with time and the properties of the pore space.

3.2 Introduction

Nanoparticles have the potential to become powerful tools for *in situ* remediation of contaminants in the subsurface environment (Zhang 2003; Elliott and Zhang 2001; O'Carroll et al. 2013; Machado et al. 2013). The exponentially increasing use of NPs in consumer products

and industrial and medical processes suggests that they may also become environmental contaminants (Tratnyek and Johnson 2006; Durenkamp et al. 2016; Patil et al. 2015). To protect valuable natural resources with, and against, NPs it is imperative that their transport in porous media be understood and that methods for detecting NPs be developed.

Nanoparticles are used for *in situ* groundwater treatment in two main applications: mobile NPs are injected to treat source zone contamination and immobile NPs are injected to treat contaminant plumes similar to permeable reactive barriers (Tratnyek and Johnson 2006). The unique properties of NPs are used to enhance the treatment of contaminants and promote the removal of contaminants from groundwater through sorption or complete degradation. Laboratory and field scale experiments have been conducted to quantify NP transport in porous media. Laboratory experiments have evaluated many different types of NPs including silver (VandeVoort and Arai 2012), fullerene (Lecoanet et al. 2004), gold and carbon nanotubes (Afrooz et al. 2016) with respect to their transport properties. Field experiments have been primarily focused on transport of nanoscale zero valent iron for remediation (Krol et al. 2013; Kocur et al. 2014; O'Carroll et al. 2013) and other NPs for oil recovery (Su et al. 2012; Son et al. 2015).

Colloid stability has been described with both classic and extended Derjaguin, Landau, Verwey and Overbeek (DLVO) theory which incorporates attractive van der Waals interactions, repulsive electrostatic double layer interactions, and, acid-base, steric and hydrodynamic interfacial forces respectively (Hoek and Agarwal 2006; Derjaguin and Landau 1993; Verwey 1947). Classic and extended DLVO theories assume physical and chemical homogeneity which are unrealistic environmental conditions. Colloid filtration theory (CFT) describes the three processes that attract a colloidal particle to a collector or grain: interception, sedimentation and

35

diffusion (Yao et al. 1971). Physicochemical properties of the aqueous solution, NPs, and porous media all have an impact on NP mobility. Nanoparticle mobility has been shown to decrease with increasing aqueous ion concentration and ionic charge (Sasidharan et al. 2014; Becker et al. 2015), clay content (Bayat et al. 2015; Cai et al. 2014; Basnet et al. 2014), pore space heterogeneity (Loveland et al. 2003; Hoek and Agarwal 2006), grain surface roughness (Benamar et al. 2007) and NP size (Benamar et al. 2007; Sasidharan et al. 2014). Nanoparticle mobility increases with increasing water velocity (Tosco et al. 2012; Sasidharan et al. 2014) and degree of water saturation of porous media (Kumahor et al. 2015a; Kumahor et al. 2015b).

Palladium NPs can act as a catalyst to enhance the removal of dissolved contaminants such as trichloroethene, and, oxyanions such as bromate, chlorate, nitrate and nitrite (Chaplin et al. 2012; Wong et al. 2009). Palladium is also used as a coating in bimetallic NPs to enhance their catalytic properties and protect them against degradation (Zhan et al. 2009). Bimetallic NPs such as nanoscale zero-valent iron coated with Pd are highly retarded in aquifer materials even when coated with stabilizing agents (Bennett et al. 2010). It is important to understand the transport of Pd NPs in porous media to determine how they can be appropriately utilized in the remediation of environmental contaminants.

Synchrotron x-ray computerized microtomography (SXCMT) uses synchrotron x-rays to penetrate a sample and collect information on the materials through which the x-ray beam has passed (Spanne and Rivers 1987). The sample is rotated and multiple two dimensional images are collected and then reconstructed into a three dimensional image of the solid, water and gas phases. Difference imaging utilizes k-edge spectroscopy and allows two images, above and below the k-edge of the element of interest, to be subtracted to give the response of that individual element. This type of imaging is non-destructive and allows time dependent

36

experiments to be conducted to illuminate pore scale NP transport (Altman, et al. 2005a; Altman et al. 2005b; Gaillard et al. 2007).

In this study, the transport of Pd NPs through three different porous media was evaluated using small-scale column experiments. The column effluent was collected and analyzed to produce traditional break-through curves (BTC). Three dimensional images of the porous media were collected using SXCMT and pore-scale data was collected at five times during each BTC for each column. These two types of data, traditional BTC and SXCMT, are integrated to provide a more comprehensive understanding of mechanisms controlling NP transport in porous media.

3.3 Materials and Methods

3.3.1 Solution Synthesis

Simulated groundwater was prepared by adding reagent grade $CaCO_3$ (3.6 mg L^{-1}) to UPW (type 1) (MilliQ system A10 water system; 18.2 MΩ cm @ 25 ^{o}C) that was bubbled with CO_2 gas followed by equilibration with atmospheric CO_2. Polymer coated Pd NPs were synthesized using a method developed by Paio et al. (2007) by dissolving 20 mL of 0.1 mol L^{-1} $KPdCl_4$ (Sigma Aldrich, Toronto, Canada) into 2 L of 20 g L^{-1} Pluronic 123 polymer solution (BASF, Ludwigshafen, Germany) and magnetically stirring for 24 hours. The polymer coating (Pluronic 123) is a nonionic symmetric triblock copolymer, with alternating hydrophobic and hydrophilic polymer blocks, that acts as a surfactant. The NPs were then washed by adding a 2:1 v/v propanol:hexane solution and centrifuging to remove the NPs from solution. The washed Pd NPs were suspended in 50 mL of 20 g L^{-1} Pluronic 123 and UPW solution.

3.3.2 Column and Packing Materials

Custom acrylic columns (Dynalab Corp, Rochester, NY) with internal diameter of 6.35 mm (¼ in.) and outer diameter of 12.7 mm (½ in.) with hose barb connections at either end, sealed with o-rings were used for NP transport experiments. Marine epoxy (LePage, Toronto, Canada) was used at the connecting point between the hose barb and the column to ensure a water tight seal. An imaging window was machined into the exterior of the column post fabrication, which decreased the outer diameter of a 5 cm length segment along the middle of the column to 9.525 mm (3/8 in.), limiting the thickness of plastic in the path of the beam to ensure maximum intensity to the sample. Sediments that were packed into the columns included aquifer sand collected at CFB Borden (split 467; Ball et al. 1990), coarse-grained silica sand (Ottawa sand; 30< mesh <25), and attapulgite clay, a magnesium-aluminum non swelling phyllosilicate clay with a needle-like structure (Zemex Industrial Minerals Inc., Attapulgus, GA). Glass wool was used as a filter at the influent and effluent ports of the column.

3.3.3 Packing and Saturation of Columns

Each column was dry packed with one of three types of sediment, 100% Ottawa sand, 100% Borden sand or a mixture containing 98% Ottawa sand and 2% attapulgite clay. The column end fittings were first packed with the glass wool and one fitting was attached to the column prior to packing. The sand or sand/clay mixture was introduced through the top of the column and the column was gently tapped to compress the sediment. The column was sealed with the top end fitting containing glass wool. O-rings were used to seal the column and marine epoxy was used on the threading to ensure no leaks would occur. Pump tubing (polypropylene (PharMed BPT™) tubing; Cole-Parmer, Montreal, Canada) was attached to either end of the column to facilitate solution input and effluent collection.

The packed columns were saturated with CO_2 gas for approximately 15 minutes to minimize residual atmospheric gases during saturation. Ultrapure water was introduced to the column with a multichannel high-precision peristaltic pump (Ismatec, Cole-Parmer) at a flow rate of approximately 1 mL min^{-1}; the columns were visibly saturated in approximately 40 minutes and were allowed to flow for 20 – 33 pore volumes (PV) after saturation. The tubing was then clamped and columns were submerged in UPW for transport to the experimental facility for tomography analysis.

3.3.4 Experimental Set Up for Column-based Transport Studies

Difference imaging was performed using SXCMT at the Argonne National Laboratory at Sector 13-BM-D in the GSECARS facility. Each column was set up in the experimental hutch on a custom imaging stand manufactured at the Science Student Machining Shop at the University of Waterloo. The imaging stand was connected to a Newport M-VP-25XA Precision Compact Linear Stage that was used to position the column in the path of the beam by translating the sample stage and a Newport URS75BPP Precision Rotation Stage to rotate the column during imaging. After arrival at GSECARS, the column was reconnected to the peristaltic pump to resume flow of UPW through the column. Each column was flushed with UPW for 10 – 17 PV prior to the experiment.

Each column was imaged at five separate times during the experiment: before NP injection, during NP injection, at full saturation of NP solution, during UPW flushing and after UPW flushing. Columns injected with NPs in a SGW solution were also flushed with UPW. Nanoparticle solutions were sonicated prior to the experiment and hand shaken directly before injection. During NP injection the peristaltic pump was stopped and was disconnected from the input tubing connected to the column. A 1 mL syringe was connected to the input tubing and was

used for the injection of NPs into the column. The pump was halted and no solution input (UPW, NP solution or SGW) was injected during imaging.

3.3.5 Tomography Data Acquisition and Preprocessing

Images at each stage of the experiment were collected above and below the Pd K-edge energy (24.50 and 24.21 keV). Each 3D image is reconstructed from 900 2D projections collected over 180º rotation of the sample stage. The beam passes through the sample and then through the scintillator which is a 250 μm leuticium aluminum garnet crystal. The scintillator converts the x-rays to visible light, which then is reflected by a mirror into a Nikon macro lens set at its minimum focal distance. A Point Grey Grasshopper3 camera with a Sony IMX174 CMOS sensor was used to capture the visible light. The field of view was 11.02 mm horizontal and 6.89 mm vertical with 1920 x 1200 pixels of resolution 5.74x5.74 μm^2.

Preprocessing and reconstruction of the projections was executed with IDL (Exelis Digital Visual Information Systems) tomography processing software developed at GSECARS (Rivers et al., 1999, 2010). Preprocessing with reconstruction corrects for the background response (flat field) collected by the sensor with no sample present, and converts two-dimensional projections into a 3-D image using filtered back-projection algorithms. The grey scale values of the voxels in reconstructed images represent the linear attenuation of the material contained within them.

After the images at each energy level are reconstructed the below edge energy image is subtracted from the above edge energy image and shifted to produce the best spatial fit of the images. This process results in a difference image where the grayscale values represent the change in linear attenuation coefficient due to the presence of Pd in each voxel.

3.3.6 Palladium Standards

Standard solutions of Pd NPs were prepared by serial dilution of the initial input solution with UPW. A bundle of capillary tubes was filled with solutions containing five known NP concentrations and imaged with SXCMT. The standards were analyzed to determine the heterogeneity of the NP solution and to understand the mass attenuation of the solutions with minimal interference from the porous media.

3.3.7 Palladium Concentration Analysis: ICP-OES

Effluent samples were collected during the experiment and solid samples were collected at the completion of the experiment. All aqueous samples were digested by adding 1 mL of 18N trace-metal grade HNO_3 to 1 mL of sample containing Pd NP. All solid samples were digested by adding an aliquot of 1 mL of UPW to 1 g of solid material collected during column disassembly, then 1 mL of 18N HNO_3 was added to digest the samples for 24 hours. Following digestion, 8 mL of UPW was added to each digestate and the samples were hand shaken and filtered with a 0.45 μm membrane and a 24 mL syringe (Nalgene). Five different Pd NP concentrations were used as a standard curve and were created by dilution of the original synthesized Pd solution of 1.15 g/L. Palladium concentrations for the digested samples were determined by inductively coupled plasma – optimal emission spectrometry (ICP-OES; iCAP 6000; Thermo Scientific).

3.4 Results and Discussion

3.4.1 Tomography Data Post-processing

Postprocessing of 3D tomography images was conducted using ImageJ (Schneider et al. 2012) and Blob3D (Ketcham 2005) successively to separate the different phases that were present in the tomography data sets. There are three phases in each tomography data set: solid, liquid, and

gas, which are present as solid (sand or clay), water (including the NP suspension), and air. Computer segmentation was utilized to separate the three phases and delineate the phase boundaries. Delineation and segmentation is a multistep process, used to overcome the noise present in the data sets.

First, a median filter was applied to the reconstructed data set to smooth the data set and reduce noise. The median filter takes the grey scale value of each voxel and replaces it with the median grey scale value of voxels in its immediate vicinity. An auto thresholding function was applied to separate the solid phase (sand or clay) from the other phases (water, NP suspension and air). This function creates a black and white binary image from an 8-bit grey scale image using a variation of the iterative intermeans auto thresholding algorithm, which uses the mean value of the four corner pixels of the image to classify the remaining pixels as either background or object. The algorithm then iteratively uses four new background pixels, closer to the object-background boundary, to reclassify each pixel and reduce noise in the binary image (Ridler and Calvard 1978). The data set was subsequently eroded twice, where a layer one voxel in width is removed from the perimeter of a group of voxels for each erosion event. Eroding the data set reduces the number of holes that are present in the solid phase and reduces the amount of voxels that are affected by refraction of x-rays close to the grain-water boundary. The data set was duplicated and inverted to provide a set where the aqueous phase was assigned pixel values of 1. These segmented data sets were then multiplied voxel by voxel with their corresponding difference image, to give a representation of the location of Pd in both aqueous and solid phases. Difference images segmented to isolate Pd response in the aqueous phase are shown in Figure 1.

The segmented data sets were analyzed to obtain porosity and average greyscale values for each slice. The porosity was obtained by taking an average of each binary slice with pore

voxels having a value of 1 and sand voxels having a value of 0 to give an approximation of the porosity in each slice. The average greyscale was converted to a Pd concentration using the following equation:

$$(3.1) \qquad C_{Pd} = \frac{\frac{\Delta A}{l} - [(\alpha_a - \alpha_b)\rho]_{water}}{(\alpha_a - \alpha_b)_{Pd}}$$

which is a derivation of the Beer-Lambert law and has been modified for application to Pd data from the equation derived for SXCMT difference imaging with Ag NPs (Molnar et al. 2014). Values for mass attenuations for water and Pd at the imaging energies (α_a, α_b) were obtained from the NIST XCOM online data base (Berger et al., 2010). The mass attenuation for water at 24.50 KeV (α_a) is 5.279×10^{-1} cm^2 g^{-1} and at 24.27 KeV (α_b) is 5.375×10^{-1} cm^2 g^{-1}. The mass attenuation for Pd at 24.50 KeV is 5.810×10^{1} cm^2 g^{-1} and at 24.27 KeV is 1.012×10^{1} cm^2 g^{-1}. The change in mass attenuation value (ΔA) is observed by the camera and is represented by the voxel grey scale value in each image. The voxel grey scale values were converted back to the ΔA value to account for the initial conversion to a 32-bit grey scale image. The segmentation and analytical algorithms were implemented using a custom ImageJ macro that is provided in the supporting information.

The segmented data sets were then used as an input into Blob3D where the software processes the data in 3D, and allows the user to segment and approve regions of interest, e.g., pores and grains, and then provides data on these 3D spaces, including volume, surface area, vertical position within the column, mean grayscale value within individual pores and other spatial information such as tilt orientation.

3.4.2 SXCMT Characterization of Porous Media

Ottawa sand and Borden sand have been characterized extensively with techniques such as sieve analysis, optical microscopy and other analytical techniques (ASTM C 778-02, 2002, Ball et al. 1990). SXCMT imaging produces a 3D representation of porous media containing information such as particle size and shape, surface roughness, and composition (Fig. 3.1). Based on SXCMT imaging, the Ottawa sand used in the experiments has a mean grain diameter of 0.7 mm, a porosity of 0.37 (Fig. 3.1). The sand grains are well rounded and have high sphericity, and are well sorted with some surface roughness and irregularities. The Ottawa sand grains are mostly uniform in composition with some Fe inclusions and Fe cement (Fig. 3.1). Previous characterization concludes Ottawa sand is composed of 99.7% quartz (ASTM C 778-02, 2002). The SXCMT analysis indicates the Borden sand grains have a mean grain diameter of 0.15 mm, a porosity of 0.25 and are sub-angular and have low sphericity. They are poorly sorted and have visible surface roughness and irregularities. Borden sand has grains of multiple compositions with many small Fe oxide grains (Fig. 3.1). Previous characterization concludes Borden sand is composed of a mixture of predominantly quartz, plagioclase, potassium-feldspar, calcite and rock fragments (Ball et al. 1990).

3.4.3 Breakthrough Curves and Retention of NPs

Nanoparticles were injected into five columns until the NP solution was visible at the imaging window which was located at approximately, but not exactly, the same height above the influent end of each column. The five columns were Ottawa – UP, Ottawa – SG, Borden – UP, Borden SG, and Ottawa + Clay – UP (Table 3.1). The input volumes ranged from as little as 2 pore volumes (PV) for the Ottawa – UP column and as large as 12 PV for the Borden – UP column (Table 3.1; Fig. 3.2). The discrepancy in the transport times required for the input of NPs to

visually arrive at the imaging window is attributed to differences in the properties of the porous media and the composition of the pore water.

For all of the column experiments, after the NPs were first visually observed at the imaging window, injection of the NP solution was continued until the entire column was visually saturated with NP. The maximum concentrations eluted from each of the columns was 0.94, 0.71, 0.55, 0.51 and 0.46 g L^{-1} for columns Borden – SG, Ottawa – SG, Ottawa + Clay – UP, Ottawa – UP, and Borden – UP, respectively (Fig. 3.2). The maximum concentrations eluted were highest in SGW columns because the SGW likely promoted the sorption of nanoparticles to grain surfaces which were likely desorbed from attachment sites when UPW was reintroduced to the columns. However, as the columns are small and the amount of effluent required to analyze for Pd concentration is relatively large (at least 1 mL equal to approximately 1 PV for each column), the resolution these samples represent is very low.

Ultrapure water was introduced into the columns after the NP solution to promote the elution of NPs from the columns. Post-injection concentrations of Pd NPs in the effluent samples returned to low concentrations in the Ottawa – UP and Borden – UP columns but remained above 40% of the injected NP concentration in Ottawa – SG, Borden – SG and Ottawa + Clay – UP columns. The NP pulse was displaced from the Ottawa – UP column rapidly, with NPs no longer visible in effluent solution at 5 PV, compared to 31 PV in the Borden – UP column. The NP pulse was eluted in approximately 1.5 times the amount of time required to inject it into the Borden – UP and Ottawa – UP columns.

The BTC for all five columns were simulated using the STANMOD CXTFIT 2.1 software package (Toride et al. 1995) assuming equilibrium transport conditions. Three different simulation conditions with varying input parameters and model assumptions were performed: (1)

solute mass is known, assumed to be the total mass input to the column, and kept constant, (2) solute mass is unknown and fitted to the data, and (3) solute mass is known, assumed to be the total mass eluted from the column, and kept constant. STANMOD CXTFIT utilizes the convection dispersion equation (CDE) as described:

(3.2) $$R\frac{\partial c}{\partial t} = D\frac{\partial^2 c}{\partial x^2} - v\frac{\partial c}{\partial x}$$

where c represents aqueous concentration (ML^{-3}), t is time (T), x is distance (L), v is the average pore-water velocity (LT^{-1}) and D is the dispersion coefficient (L^{2}T^{-1}). The retardation factor, represented by R, is a dimensionless parameter which, conceptually, is the relative velocity of the transported species of interest (Pd NPs) compared to a conservative tracer. The retardation factors and dispersion coefficients were obtained by inverse modelling of the experimental effluent BTC data, using normalized concentrations and dimensionless time, to optimize parameter fitting using non-linear least-squares. Input parameters included the pulse duration and concentration for a third type, flux-averaged, input. More advanced analysis assuming non-equilibrium conditions is not included because the simulations would be poorly constrained due to the limited experimental data.

Dispersion coefficients, obtained by simulation 1, for the five columns decreased from largest to smallest in the following order, Ottawa – UP, Borden – UP, Ottawa + Clay – UP, Ottawa – SG, Borden – SG, with coefficients of, 9.99, 2.95, 0.306, 0.245 and 0.121 respectively (Table 3.1; Fig. 3.2). Dispersion coefficients, obtained by simulations 2 and 3, ranged from 4000 – 0.002 (Table 3.1; Fig. 3.2). The differences among the modelled dispersion coefficients for the columns is attributed to the low sampling resolution, especially for Ottawa + Clay – UP, Ottawa – SG, and Borden – SG column effluent. For these columns, the final effluent Pd NP

concentrations were > 40% of the initial input concentration, resulting in poorly constrained simulations, particularly on the falling limb of the NP pulse (Fig. 3.2).

Retardation factors, obtained by simulation 1, for the five columns decreased from: Borden – UP, Ottawa – UP, Ottawa + Clay – UP, Borden – SG, Ottawa – SG with factors of, 33, 9.18, 9.18, 8.61, and 3.26 respectively (Table 3.1; Fig. 3.2). The retardation factors obtained by simulation 2 decreased from: Borden – SG, Borden – UP, Ottawa + Clay – UP, Ottawa – UP, and, obtained by simulation 3 from: Ottawa + Clay – UP, Borden – UP, Borden – SG, Ottawa – SG, Ottawa – UP. In each simulation, the Pd NPs were more heavily retarded in Borden sand than in Ottawa sand. The modelled retardation factors for Borden sand columns are higher than Ottawa sand columns with the same NP solution. However, because the simulations for the SGW columns (Borden – SG and Ottawa – SG) were poorly constrained the retardation factors for these columns cannot be reliably compared to the UPW results.

The equilibrium transport model is not considered to be an adequate model for determining the parameters needed to describe NP transport because NPs can form a colloidal dispersion and thermodynamic equilibrium is not reached regardless of the stability of NPs in a homogenous mixture at the macro scale (Praetorius et al. 2014). However, in this study the equilibrium transport model was used comparatively among the experiments presented. Trapezoidal integration of the breakthrough curve data was used to determine the mass of NPs eluted from the column independently of a transport model (Fig. 3.3). The transport parameters obtained using the equilibrium method should not be directly used to predict the fate of, or assess the environmental risk associated with Pd NP (Praetorius et al. 2014).

Retention of NPs was visually observed in the columns as a dark zone when compared to the original column before NP injection. Nanoparticle retention in the columns was confirmed

using sediment digestion procedures at the conclusion of the experiments and the results were compared to the mass of NPs that were eluted from the column. Mass-balance fractions were determined through digestions of sediment samples collected from the columns and digestion of effluent samples, subsequently analyzed by ICP-OES. The total mass of Pd NPs was calculated from the Pd NP injection volume and the Pd NP concentration in the input solution. The sorbed mass of Pd NPs was calculated from the Pd NP concentration from the sediment digestion and the total mass of sediment present in each column. The eluted mass of Pd NPs was calculated from the Pd NP concentration and volume of all effluent collected from the respective columns.

Sand collected from the Ottawa-UP column had a greater ratio of NPs eluted to NPs retained with values of greater than 28:1 (Fig. 3.3). Sand from the Borden - UP columns retained more NPs with ratios of mass eluted to mass retained of < 13:1 and as high as 1:1. The percentage of NPs not recovered ranged from 6 to 60%, which could be due to NPs retained in tubing or on column materials, or due to NP loss during sampling. The absolute masses of NPs that were unaccounted for increased as sampling time increased for columns containing the same porous media (Fig. 3.3). Unaccounted NPs were likely lost during sampling or were retained in the column apparatus. The retention ratios in these columns are consistent with previous studies that suggest NPs are retained in porous media with lower porosity, higher grain-surface areas, and more complex geochemical surface properties (e.g., Loveland et al. 2003).

Mass determined through trapezoidal integration of the BTC and the mass of the eluted fraction determined through the digestion of effluent samples are within 30% for all columns, indicating the BTC analysis and mass balances are consistent (Table 3.1). Total mass (M_T) calculated from simulations 1, 2 and 3, are 44%, 26% and 9% different from the mass of the eluted fraction, respectively, for Ottawa – UP and are 35%, 10% and 6%, respectively, for

Borden – UP (Table 3.1). Simulation 1 assumes full elution of the NP and that the mass of NP input to the column is equal to M_T calculated from the BTC (Table 3.1). Simulations 2 and 3 are most representative of transport of the mobile fraction of the NPs.

3.4.4 Imaging of NP Transport Experiments by SXCMT

3.4.4.1 Palladium NP Standard Solutions

Each 3D image of the Pd standards determined by SXCMT contained 93,800,000 water voxels. The standard solutions were used to compare concentrations obtained from the corrected synchrotron Pd response to those obtained from direct analysis by ICP-OES to assess whether there was a correlation between the two types of measurement. Palladium NPs were detected by the SXCMT technique and are linearly correlated ($R^2 = 0.99$) with concentrations determined by direct analysis of Pd in the aqueous standards (*i.e*., ICP-OES; Fig. 3.4). The best fit of the slope deviates from unity by 180% and has a y-intercept of -0.22. The SXCMT concentration overestimated the Pd concentration determined through direct analysis. The Pd concentration could be overestimated by SXCMT technique by signal discrepancy between the x-ray attenuation captured by the camera and the true x-ray attenuation that occurred within the column (Molnar et al. 2014). Alternatively, the Pd concentration determined through direct analysis of the standards could be underestimated through sample loss during sample preparation or incomplete digestion. This result differs from that of Molnar et al. (2014) who observed that in porous media the Pd concentrations detected by SXCMT were lower than values determined by extractions.

3.4.4.2   Transport of NPs through Porous Media

Palladium NP transport experiments were conducted on five columns (Table 1) and 3D images were collected during five critical stages during the NP BTC: (1) pre-monitoring, (2) rising limb, (3) peak, (4) falling limb, and, (5) post-monitoring. The pre-monitoring and post-monitoring images are denoted as initial and final images, respectively. The images were analyzed using two methods which analyze the aqueous phase present in different representative elemental volumes (REV). Slice-wise Pd response represents a section of pore water in one horizontal plane. Pore-space Pd response represents a section of pore water in one individual pore.

3.4.4.2.1   Slice-wise Pd Response

Three dimensional images were analyzed by grouping voxels of the same phase that occur on the same horizontal plane, referred to slices, that can be collectively stacked together to create a 3D image. Each slice was analyzed separately to determine the properties within the column: Pd concentration and porosity. Each slice was 5.74 μm thick and contained 416,025 voxels in a 3.7 x 3.7 mm square cropped from the middle of the column. All images of each column contained 1200 horizontal slices.

The porosity of the packed sediment is an important parameter in the image analysis but also for understanding NP transport. The porosity varied from 0.31 to 0.45, 0.35 to 0.42, and 0.19 to 0.35, in the Ottawa – UP, Ottawa + Clay – UP, and, Borden – UP column respectively (Fig. 5). Ottawa sand had a pore network with large and well connected pores, whereas the Borden sand pore network included smaller pores that were poorly connected (Fig. 3.1). The 3D images for each column experiment were analyzed separately and both Ottawa – UP and Ottawa + Clay – UP columns showed good agreement between the calculated porosity values, indicating

that the sand grains did not compress or move appreciably over the duration of the experiments. This agreement also indicates that the column was not moved during imaging and that comparisons between the images are valid. The calculated porosity decreased over the duration of the experiment in the five images analyzed for Borden – UP which may be due to consolidation of the Borden sand over the duration of the experiment or may be due to the vertical movement of the column between the collection of images.

Each slice is a thin section that contains sections of multiple pores spaces that are averaged to obtain the overall Pd response. This response is correlated to the average concentration of Pd present in the aqueous solution by the modified Beer-Lambert law (Eq. 3.1). This information is analogous to analyzing a 32 nL aliquot of pore water, which is approximately 0.003 PVs. The resolution of the slice-wise data is much greater than the effluent analyzed to obtain the BTCs which contained multiple PVs in each sample. The drawback of this technique is that it averages the Pd response in slices that contain many different pore spaces that may have different Pd responses, and this information is obscured by averaging.

The initial, pre-monitoring image, where no NPs were injected into the columns (Fig. 3.5), contains slices which all have negative calculated Pd concentrations. The Pd concentration calculated from the initial image demonstrates the method because there is no Pd present in the column at this time. The saturated image, where NPs were injected to obtain complete visual column saturation, contains slices that on average have a calculated Pd concentration of 1.5 g L^{-1}. The difference between the initial image and the saturated image is a factor of two increase in calculated Pd response. The leaving image, captured during the reintroduction of UPW to the column, mirrors the saturated image and it is likely that only minimal flushing of the void spaces had occurred at this time. The final image, collected when the UPW had been pumped until the

NP concentration in the column effluent was visibly undetectable, contains slices similar to the calculated Pd concentration of the initial images. The Pd NPs were likely removed from the main pore spaces in the Ottawa – UP and Ottawa + Clay – UP columns, while some NPs may have been retained on the grain surfaces but remained on the grain-water boundary, invisible to the SXCMT technique.

The SXCMT difference image technique cannot be used to visualize phase boundaries because refraction occurs as the x-ray beam crosses the boundary (Cloetens et al. 1999; Molnar et al. 2014). The refraction of the beam causes intensity modulation in the resulting projections and accurate calculated Pd concentrations cannot be obtained from the area directly surrounding phase boundaries. The exact size of this boundary is determined by the sample to scintillator distance, the energy of the beam, and the composition and density of the phases in the beam path, but has been calculated in similar sediments to be 18.1 μm from the grain-water boundary (Molnar et al. 2014). This distance represents the width of 3,620 NPs, which have a diameter of 5 nm. As a consequence, a very large aggregate of NPs adsorbed to the grain surface would be invisible using SXCMT difference imaging.

The grain-water boundary has a large role in the fate and transport of NPs in porous media. Interactions among the NPs, grain surfaces and aqueous solutions determine whether the NPs will be attracted to and immobilized by the grain or remain in solution and transported out of the column in the effluent. Any Pd NPs retained on the Ottawa sand grain surfaces or near the grain surfaces would not be apparent in the Pd concentrations calculated from the SXCMT difference imaging. However, there was little visual evidence of NP retention on the grain surfaces in the Ottawa sand columns (Ottawa – UP, Ottawa – SG, and Ottawa + Clay – UP) and the extractions of the solid phase of the column was consistent with the visual observation.

During unpacking the Ottawa sand columns, the sediment appeared similar to freshly washed Ottawa sand. After digestion the mass of Pd present on the sand grains from the Ottawa – UP column was only 1% of the total mass of Pd that had been injected into the column, 39% was eluted from the column, leaving 60% was unaccounted for. It is unlikely that the 60% that was unaccounted for was retained on the grains because it represents approximately 0.7 g L^{-1} of Pd NPs which have a distinct dark grey colour that would have been observed during unpacking.

Difference imaging utilizing SXCMT and processed using a slice-wise approach indicates that this technique can be used to observe the change in Pd NP concentration over the duration of a transport experiment. The amount of pore space specific information is limited in this data analysis method.

3.4.4.2.2   Pore-Space Pd Response

Separating the 3D images obtained from SXCMT difference imaging by spatial connection into separate pore spaces allows the data to be analyzed for properties of pore spaces and Pd concentration. Images segmented with ImageJ using the previously described techniques were used as input for the Blob3D program as it cannot perform data set multiplication, where binary phase data sets are multiplied by the difference image data sets to isolate the aqueous phase. Due to the input requirements for images, the Blob3D calculated Pd concentrations are represented as Pd response, which is a relative measure derived from the normalization of the SXCMT calculated Pd concentration. Blob3D was used to separate the aqueous phase into separate spatial sections referred to as pore spaces.

Each pore space is defined by the grains that surround it, with the edges of a pore space either being a grain – water phase boundary or a pore throat. A pore throat is a narrow channel between two or more grains that are not in contact with each other in the vicinity of the pore

53

throat (Dong and Blunt 2009). Understanding Pd response in relation to pore spaces is more direct in terms of fluid flow and associated transport of particles through porous media.

Pore spaces are delineated in Blob3D by using a computer algorithm that uses the aqueous phase and removes one voxel from the outer surface of the phase. The pore throats subsequently become thinner and after many iterations disappear to leave separated pore nucleuses. The pore nucleuses are assigned a unique identifier. A separate computer algorithm reverses the process and adds back a layer one voxel thick to the outer surface of the pore nucleuses. The voxels that are added back to the pore nucleuses are also associated with the unique identifier of the individual pore. This process is repeated until two pores spaces meet or the voxels meet the aqueous phase boundary and the aqueous phase is completely separated into unique pores. A 3D representation of this segmentation is created, in which each unique pore space is assigned a colour to distinguish pore spaces from one another and visually define the pore-space boundaries (Fig. 3.6).

The vertical position of the center axis, the surface area, and the volume of the pore, for each individual pore in a subset of images collected for the Ottawa + Clay – UP column, was calculated using Blob3D. Segmented slices, that had minimal imaging artifacts in a continuous section of slices over the five pseudo-temporal images in the experiment, were identified. The sets of images were used as input for Blob3D. The effect of the pore properties on the transport of NPs through the porous media was visualized with these parameters.

In a 2.2 mm section of the Ottawa + Clay – UP column, detectable Pd responses were observed in an average of 204 pore spaces in each temporal image. The average Pd response increased from the initial image, through the front image, to the saturated image and then decreased through the leaving image to return to a Pd response below zero in the final image

(Fig. 3.7). The average Pd response in the saturated image for the pore-space analysis and the slice-wise analysis was 1.57 and 1.39 respectively (Fig 3.5, 3.7), indicating the analysis techniques produce comparable results. The volume, surface area and vertical position of the center axis of the pore spaces ranged from 1500 μm^3 – 0.46 mm^3, 640 μm^2 – 9.3 mm^2, and, 65 μm – 2.2 mm, respectively. The Pd response in the saturated image ranged from -3.75 – 7.96 for the pores with volumes below the median volume of 0.033 mm^3 and ranged from 1.15 – 3.04 for the pores with volumes above 0.033 mm^3. Similar trends were observed for all images (initial, front, saturated, leaving and final) for both volume and surface area (Fig 3.7). The smaller range of Pd responses for pores with volumes above 0.033 mm^3 is likely due to the larger number of voxels that are used to determine the Pd response reducing the influence of artifacts and edge effects. The vertical position of the center was determined and shown to have no visible influence on Pd response (Fig. 3.7). No vertical trend was identified along the length of the column, likely due to the limited thickness of the section (2.2 mm).

Nanoparticle detachment from grain surfaces may happen more slowly than attachment, as observed for virus transport (Stimson et al. 2010). Nanoparticles may leave pores because of preferential flow paths which are related to the properties of the pore matrix and pores themselves (Phenrat et al. 2010). In the pore-space analysis the spread of the distribution of Pd concentrations in the pores relative to their surface area and volume increases from the pre-monitoring, rising limb and peak images, to the falling limb image (Fig. 3.7). This spread is likely caused by the release of previously sorbed NPs from grain surfaces and transported out of pores characterized by higher pore velocities due to preferential flow paths. The 3D analysis of SXCMT difference imaging could be used to understand where and why NP transport deviates from fluid flow through the addition of pore-scale flow simulations (Molnar et al. 2016).

55

3.5   Conclusions

Palladium NPs can be transported through porous media and may be used in remediation studies. Complete recovery and reusability is a critical aspect of their implementation in groundwater remediation systems. This study indicates that NP transport is more heavily retarded in Borden sand compared to Ottawa sand and in simulated groundwater compared to ultrapure water. The concentration of Pd NPs can be calculated for pore spaces in 3D using SXCMT difference imaging. The spread of Pd NP concentration with respect to pore space, surface area, and volume increases as pores get smaller. Combining SXCMT data with modeling can be a powerful tool for determining transport parameters of new and emerging nanoparticles, and understanding pore-scale properties of nanoparticle transport especially when combined with mass-balance calculations.
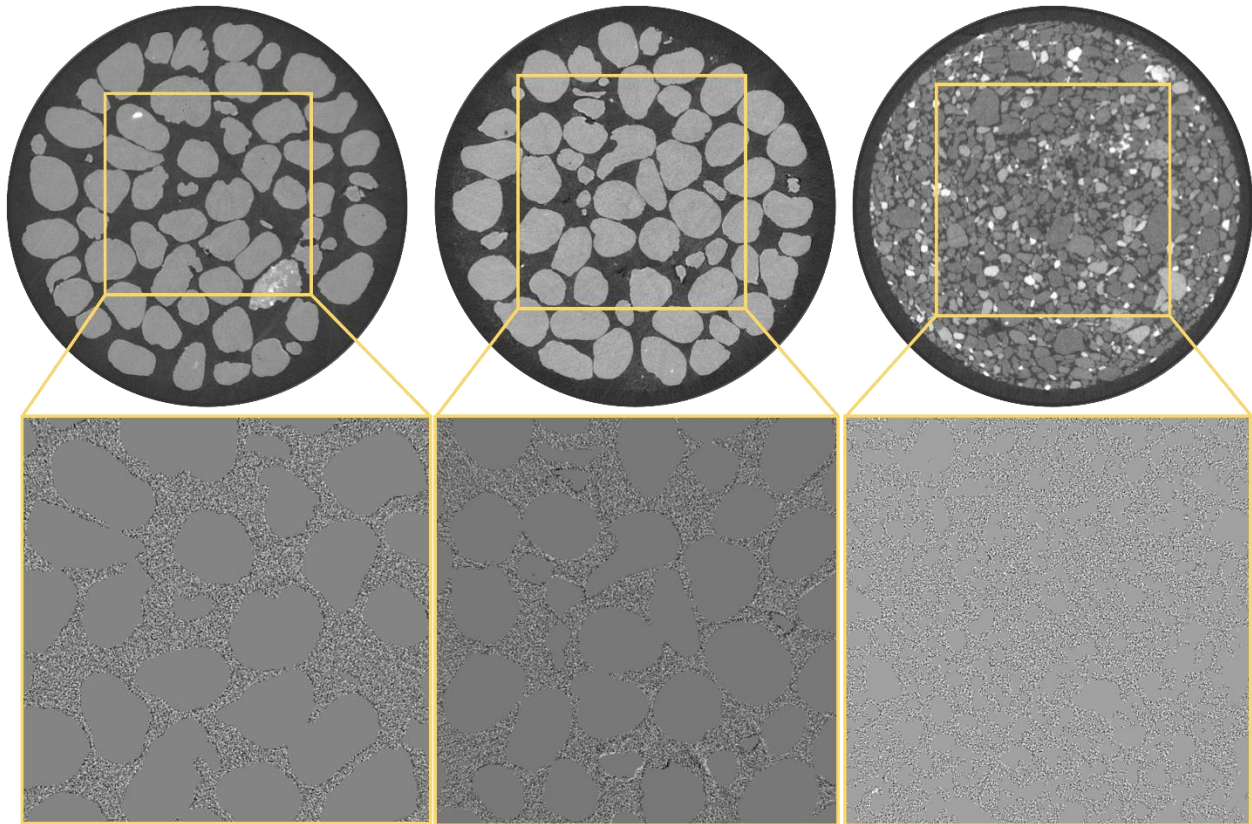
Figure 3.1 *Top row:* Reconstructed SXCMT images of (from left to right) Ottawa sand, Ottawa sand with clay and Borden sand. *Bottom row:* Processed SXCMT difference images with the segmented grains removed from the data.
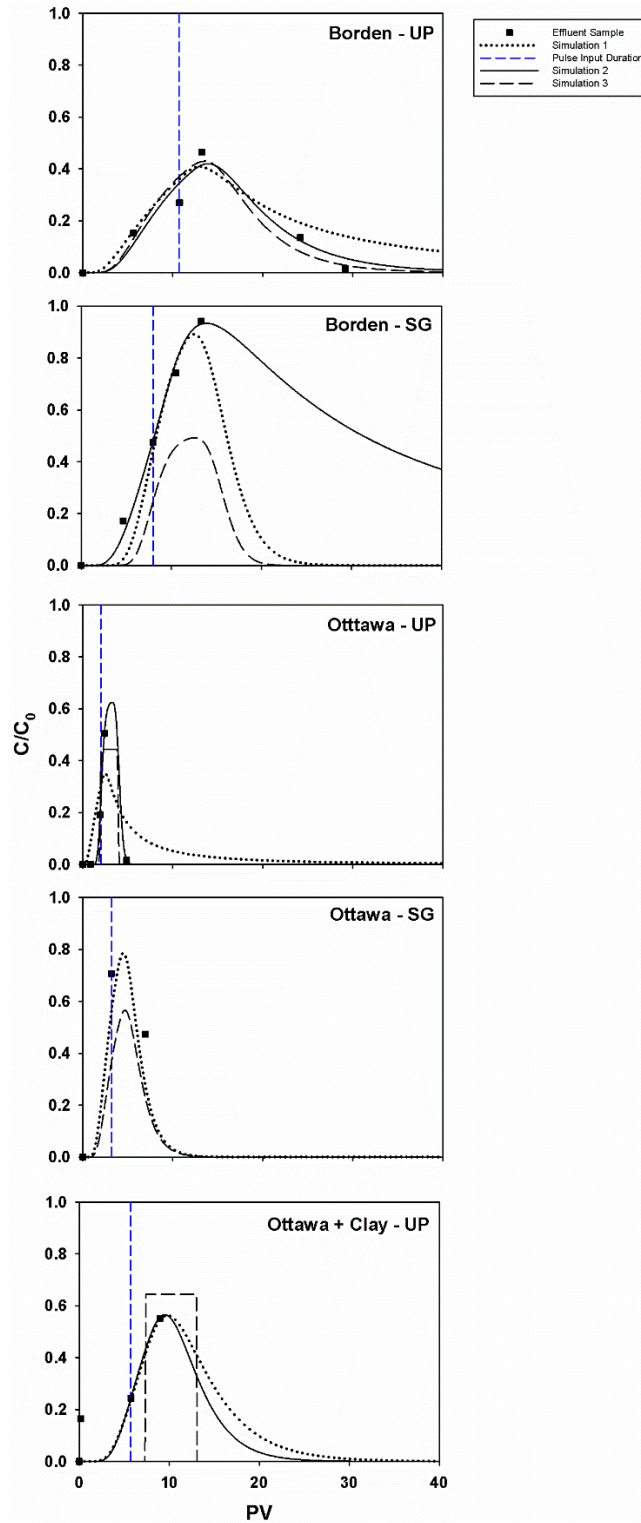
Figure 3.2 Break-through curves fitted with equilibrium CDE analytical solution (CXTFIT STANMOD 2.1) for transport of Pd NP in all five experimental columns.
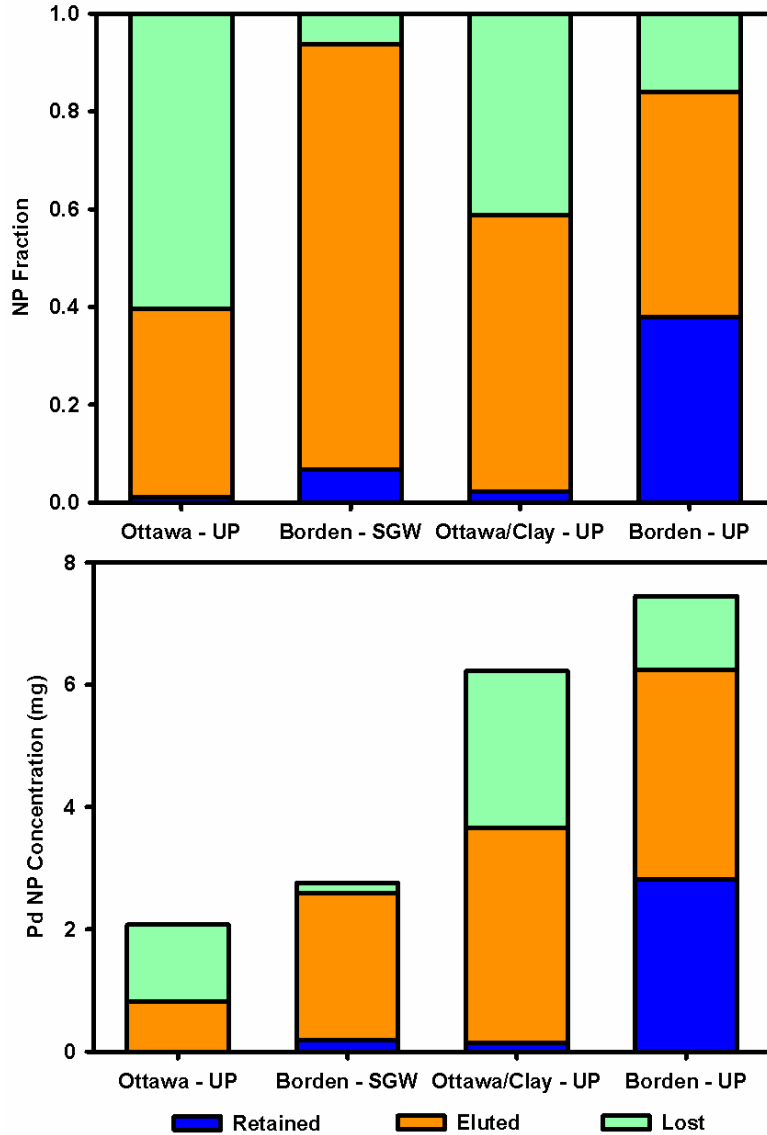
Figure 3.3. Mass balance diagrams for four of the column experiments (Borden – UP, Borden – SG, Ottawa – UP, and, Ottawa – SG). Each stacked bar graph represents the fraction of NPs that were retained in the column, eluted from the column and unrecovered (lost). *Top:* Each mass balance totals to 1. Columns containing Borden sand had eluted to retained ratios of less than 13:1, and as high as 1:1, while columns with Ottawa sand had ratios greater than 28:1. The percentage of NPs lost ranged from 6 to 60. *Bottom:* Mass balances expressed in absolute Pd NP mass.
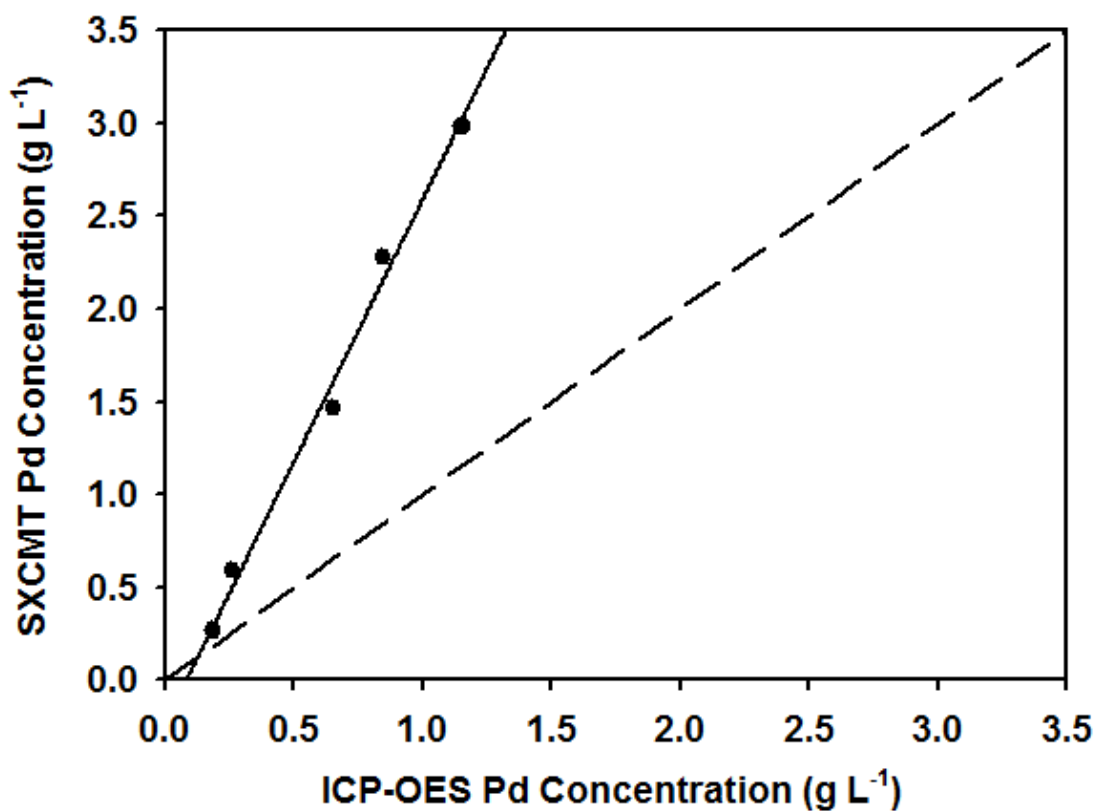
Figure 3.4. A calibration curve to compare synchrotron x-ray computerized microtomography (SXCMT) derived aqueous Pd concentrations to the concentrations from ICP-OES analysis after aqueous sample digestion. The concentrations are linearly correlated with a regression fit described by f(x)=2.80x-0.22 with an R^2 value of 0.99.
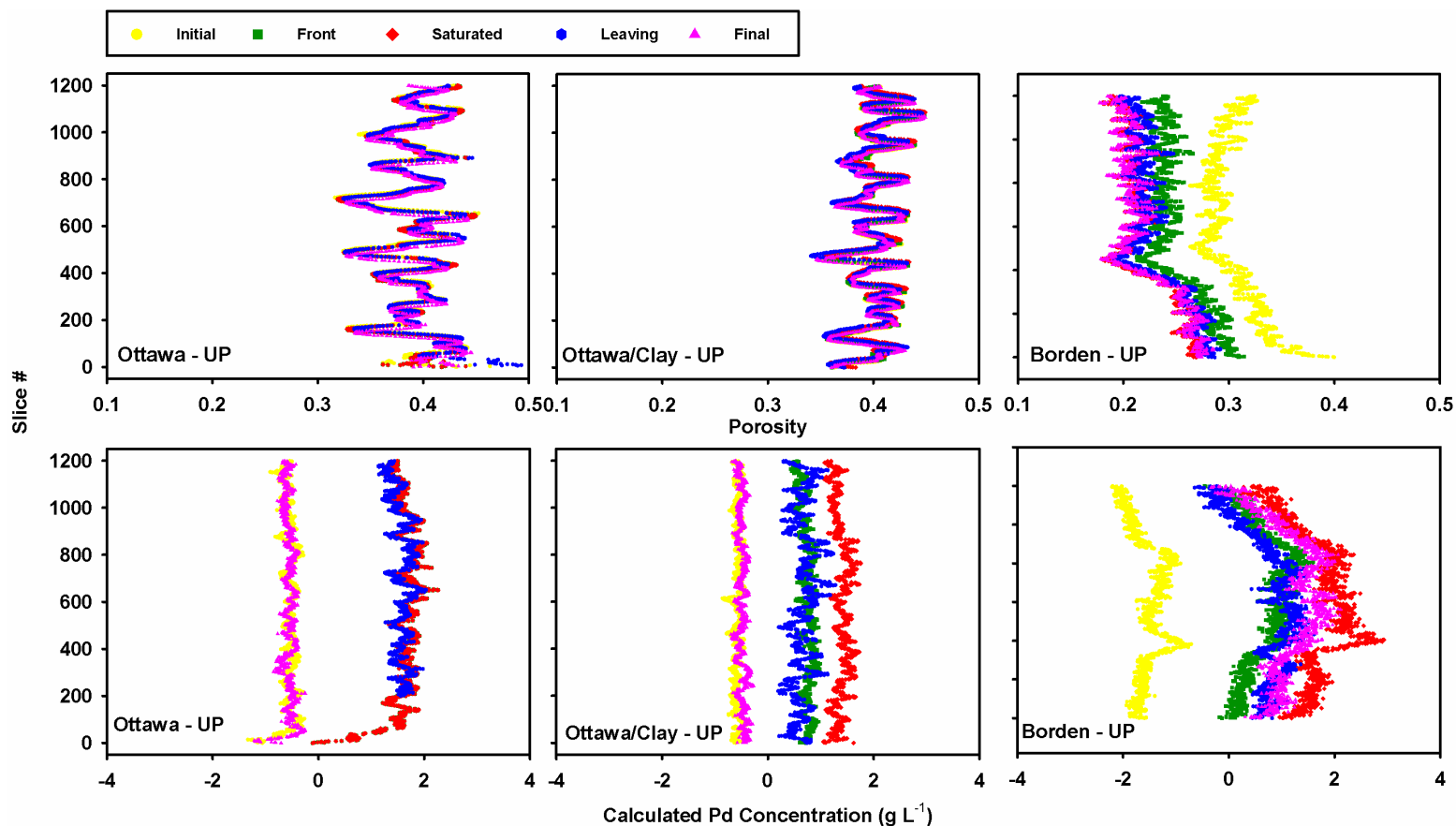
Figure 3.5 Slice-wise data for Ottawa – UP, Ottawa + Clay – UP and Borden – UP *Top row:* The porosity of a series of two dimensional (2D) images of a column packed with Ottawa sand is plotted against it position along the vertical axis of the column, represented by slice number. The porosity varies between 0.31 and 0.45. There is a good agreement between individual images taken at different time points during the experiment. *Bottom row:* The average Pd response in the aqueous portions of each 2D slice was measured and plotted against the slices vertical position along the column. The Pd response is below zero in the initial images, before NP injection. The Pd response is higher after the Pd NPs have been injected into the column. The final image after the Pd NPs have been flushed out of the column.
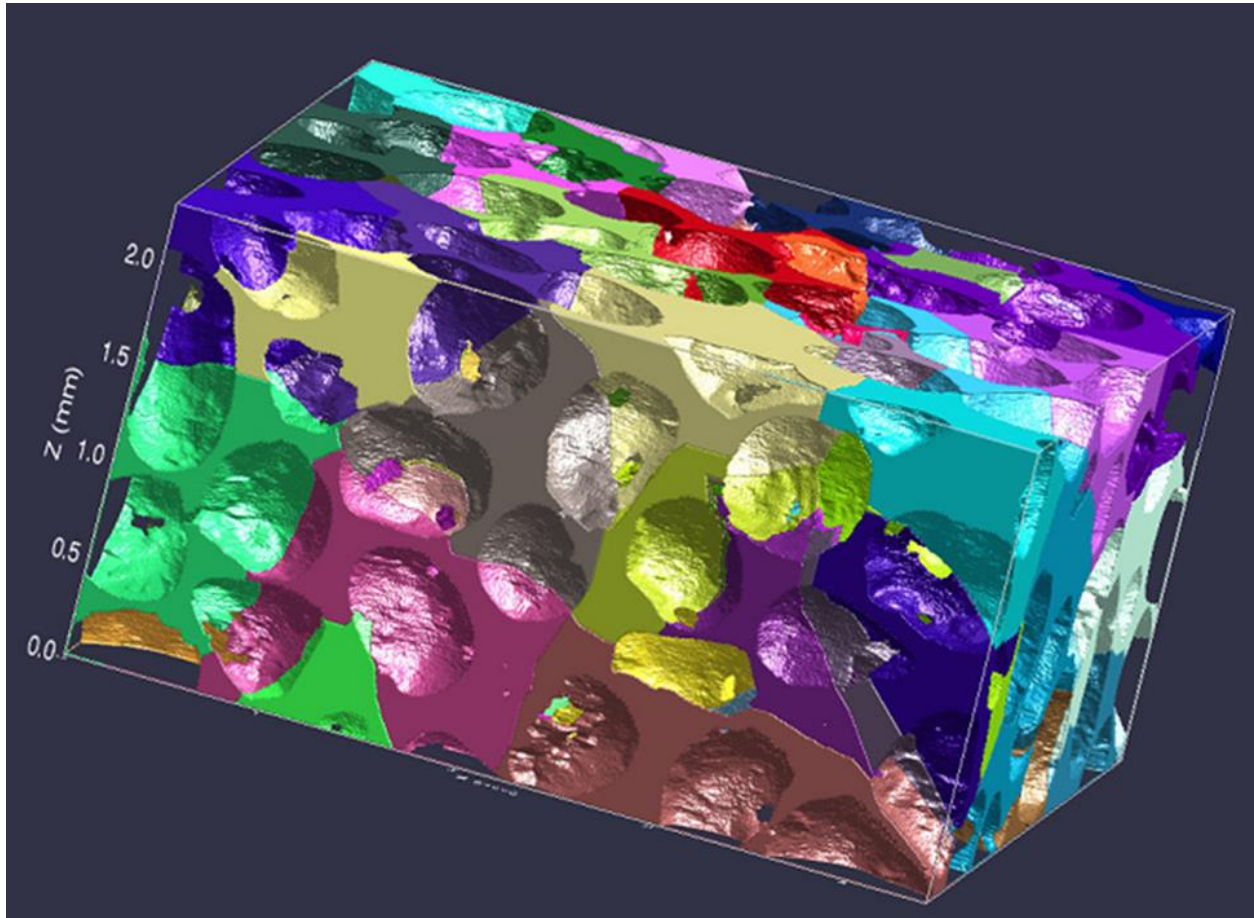
Figure 3.6. A 3D visual representation of segmented pore spaces. Each colour represents one unique pore space.
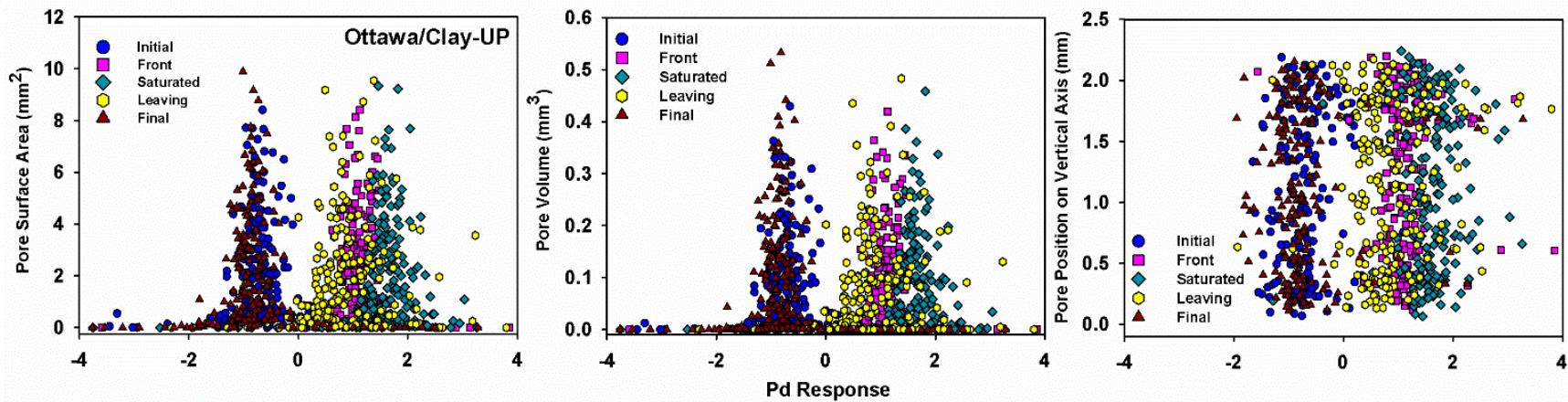
Figure 3.7. Palladium response of pore spaces in an approximately 2.2 mm three dimensional (3D) section of the Ottawa + Clay – UP column plotted against the volume of each individual pore space. Five time points corresponding to five data sets or 3D images are plotted together to show the Pd NP concentration in the pores over the duration of the Pd NP pulse injection.

Table 3.1 Description and type of data collected for each column experiment. The BTC data was inversely modelled using CXTFIT STANMOD 2.1 and three different simulations with varying input parameters and model assumptions: (1) solute mass is known, assumed to be the total mass input to the column, and kept constant, (2) solute mass is unknown and fitted to the data, (3) solute mass is known, assumed to be the total mass eluted from the column, and kept constant.

Name (Description)	Pulse Length (PV)	Mass Input (mg)	Mass Eluted (mg)	Model	Break-through Curve D	Break-through Curve R	Break-through Curve M_T (mg)	Mass Balance	Slice-wise Analysis	Pore-space Analysis
Ottawa-UP (100% Ottawa sand, saturated with UPW)	2.1	2.07	0.80	TI	--	--	0.98	Yes	Yes	--
				1	9.99	9.18	2.06			
				2	0.086	2.11	1.35			
				3	0.002	1.92	0.96			
Ottawa-SG (100% Ottawa sand, saturated with SGW)	3.2	1.72	2.18	TI	--	--	1.80	--‡	Yes[†]	--
				1	0.245	3.26	1.78			
				2	--	--	--			
				3	0.225	3.44	1.25			
Borden-UP (100% Borden sand, saturated with UPW)	10.7	7.45	3.43	TI	--	--	4.19	Yes	Yes	--
				1	2.95	33.0[†]	7.15			
				2	0.49	10.9	4.21			
				3	0.40	9.21	3.90			
Borden-SG (100% Borden sand, saturated with SGW)	8.0	2.76	2.40	TI	--	--	1.87	Yes	Yes[†]	--
				1	0.121	8.61	2.73			
				2	137	2769	7.54			
				3	0.054	8.08	1.36			
Ottawa + Clay-UP (98% Ottawa sand and 2% Attapulgite Clay, saturated with UPW)	5.7	6.23	3.51	TI	--	--	2.72	Yes	Yes	Yes
				1	0.306	9.18	6.35			
				2	0.212	7.82	5.23			
				3	4000	124	3.99			

TI is trapezoidal integration, M_T is the total mass (mg) as $\frac{dC}{dt}$, D is the diffusion coefficient (cm^2 PV^{-1}), R is the retardation (-), Mass eluted (mg) was measured by ICP-OES.

[†] Data not presented

‡Not included because of limited samples

Chapter 4:

Conclusions

4.1   Summary of Findings

Emerging environmental contaminants represent a broad suite of compounds with many aspects that require scientific exploration. Previous research has explored the presence, fate, and remediation of a wide variety of emerging contaminants. Specifically, artificial sweeteners are found frequently in anthropogentically affected environments and have been proposed as tracers for waste water in groundwater and surface water (Van Stempvoort et al. 2011). Nanoparticles have been identified as a tool for remediation of contaminants through sorption and degradation and as potentially harmful contaminants (Patil et al. 2015; Lien and Zhang 2001). Results from this thesis contribute to the understanding of artificial sweetener storage in simulated groundwater, compatibility of sampling materials with artificial sweetener compounds, Pd nanoparticle transport in various porous media and synchrotron x-ray computerized microtomography for studies of Pd nanoparticle detection and quantification in porous media.

The main findings from Chapter 2, Storage and Preservation of Artificial Sweeteners in Groundwater Samples, provide guidance to define an appropriate length of storage time and preservation techniques to allow confidence in measured artificial sweetener concentrations after sample collection from field sites. Aqueous samples with groundwater matrices and no dissolved organic carbon, collected for the determination of artificial sweetener concentrations, can be kept for up to 241 days (approximately 8 months). Aqueous samples collected for the determination of artificial sweetener concentrations should not be acidified and stored at room temperature (25 ºC). The artificial sweetener concentrations were stable at 289 days (9.5 months) in aqueous

solutions in contact with all tested sampling materials (polytetrafluoroethylene (Teflon™) tubing, polypropylene (PharMed BPT™) tubing, styrene-ethylene-butylene co-polymer (MasterFlex™) tubing, polyamide (Nylon), polyvinylchloride (PVC), aluminum and stainless steel) with the exception of steel. Aqueous samples collected for the determination of artificial sweetener concentration should not remain in contact with steel for extended periods of time

The main findings from Chapter 3, Transport of Pd NPs in Porous Media of Varying Grain Size with Synchrotron X-Ray Computed Tomography, are focused on integrating traditional breakthrough curve and mass balance analysis with a 3D imaging technique. The experimental observations suggested that Pd NP transport is more retarded in Borden sand than in Ottawa sand and is more retarded in SGW than in UPW. Palladium NP concentrations can be calculated by SXCMT difference imaging and the Pd NP concentrations determined by SXCMT can be interpreted in 3D space. Palladium NP concentration increases in variance as pore space volume and surface area decrease, and Pd NP concentration increases in variance with respect to pore volume and surface area on the falling limb of the breakthrough curve.

4.2   Future Directions

Artificial sweeteners can be useful as tracers of anthropogenic waste water in groundwater and surface water. Investigating the potential for artificial sweetener degradation by bacteria present in groundwater would be beneficial to determine interferences with utilizing artificial sweeteners as tracers. Understanding artificial sweetener degradation would provide insights into possible persistence in the environment and to develop remediation systems if artificial sweeteners became recognized as harmful to human health or the environment. The implications of dissolved organic matter/carbon on the storage and preservation of artificial sweeteners in aqueous samples are important to understand to provide further guidance for environmental

sampling. Synchrotron X-Ray Computerized microtomography(SXCMT) is a powerful tool that can non-destructively image a column and detect nanoparticles (NPs) during transport. However, SXCMT cannot currently resolve meaningful information for NP transport at phase boundaries. To improve how NP transport is understood it would be ideal to investigate techniques for quantitatively observing phase boundaries non-destructively during transport experiments to understand attachment and detachment processes that control NP transport. In the future, modeling should also be coupled with SXCMT data to validate conceptual models of NP transport under many different environmental conditions.

References

Afrooz, A.R.M.N., Das, D., Murphy, C.J., Vikesland, P., Saleh, N.B., 2016. Co-transport of Gold Nanospheres with Single-Walled Carbon Nanotubes in Saturated Porous Media. *Water Research* 99(1), 7–15. doi:10.1016/j.watres.2016.04.006.

Altman, S.J., Peplinski, W.J., Rivers, M.L., 2005. Evaluation of Synchrotron X-Ray Computerized Microtomography for the Visualization of Transport Processes in Low-Porosity Materials. *J. Contam. Hydrol..* 78(1), 167–83. doi:10.1016/j.jconhyd.2005.05.004.

Altman, S.J., Rivers, M.L., Reno, M.D., Cygan, R.T., Mclain, A.A., 2005. Characterization of Adsorption Sites on Aggregate Soil Samples Using Synchrotron X-Ray Computerized Microtomography. *Environ. Sci. Technol.* 39(8), 2679–85.

Ball, W.P., Buehler, C.H., Harmon, T.C., Mackay, D.M., Roberts, P.V., 1990. Characterization of a Sandy Aquifer Material at the Grain Scale. *Journal of Contaminant Hydrology* 5(1), 253–95.

Bartram, J., Mäkelä, A., Mälkki, E., (1996). "Chapter 5: Field Work and Sampling". In Water Quality Monitoring - A Practical Guide to the Design and Implimentation of Freshwater Quality Studies and Monitoring Programmes (0-419). Geneva: World Health Organization.

Basnet, M., Di Tommaso, C., Ghoshal, S., Tufenkji, N., 2014. Reduced Transport Potential of a Palladium-Doped Zero Valent Iron Nanoparticle in a Water Saturated Loamy Sand. *Water Research* 68(1), 354–63. doi:10.1016/j.watres.2014.09.039.

Bayat, A.E., Junin, R., Mohsin, R., Hokmabadi, M., Shamshirband, S., 2015. Influence of Clay

Particles on Al2O3 and TiO2 Nanoparticles Transport and Retention through Limestone Porous Media: Measurements and Mechanisms. *J Nanopart Res* 17(5), 218-32. doi:10.1007/s11051-015-3031-4.

Becker, M.D., Wang, Y., Paulsen, J.L., Song, Y-Q., Abriola, L.M., Pennell, K.D., 2015. In Situ Measurement and Simulation of Nano-Magnetite Mobility in Porous Media Subject to Transient Salinity. *Nanoscale* 7(3), 1047–57. doi:10.1039/C4NR05088F.

Benamar, A., Ahfir, N-D., Wang, HQ., Alem, A., 2007. Particle Transport in a Saturated Porous Medium: Pore Structure Effects. *C R Geoscience* 339(10), 674–81. doi:10.1016/j.crte.2007.07.012.

Bennett, P., He, F., Zhao, D., Aiken, B., Feldman, L., 2010. In Situ Testing of Metallic Iron Nanoparticle Mobility and Reactivity in a Shallow Granular Aquifer. *J. Contam. Hydrol.* 116(1–4), 35–46. doi:10.1016/j.jconhyd.2010.05.006.

Berger, M.J.; Hubbell, J.H.; Seltzer, S.M.; Chang, J.; Coursey, J.S.; Sukumar, R.; Zucker, D.S.; Olsen, K. NIST XCOM: Photon Cross Sections Database. http://www.nist.gov/pml/data/xcom/index. cfm (accessed Dec 29, 2013)

Berset, J-D., Ochsenbein, N., 2012. Stability Considerations of Aspartame in the Direct Analysis of Artificial Sweeteners in Water Samples Using High-Performance Liquid Chromatography–tandem Mass Spectrometry (HPLC–MS/MS). *Chemosphere* 88(5), 563–69. doi:10.1016/j.chemosphere.2012.03.030.

Buerge, I.J., Buser, H-R., Kahle, M., Muller, M.D., Poiger, T., 2009. Ubiquitous Occurrence of the Artificial Sweetener Acesulfame in the Aquatic Environment : An Ideal Chemical

Marker of Domestic Wastewater in Groundwater. *Environ. Sci. Technol.* 43(1), 4381–85.

Cai, L., Tong, M., Wang, X., Kim, H., 2014. Influence of Clay Particles on the Transport and Retention of Titanium Dioxide Nanoparticles in Quartz Sand. *Environ. Sci. Technol.* 48(13), 7323–32. doi:10.1021/es5019652.

Chaplin, B.P., Reinhard, M., Schneider, W.F., Schuth, C., Shapley, J.R., Strathmann, T.J., Werth, C.J., 2012. Critical Review of Pd-Based Catalytic Treatment of Priority Contaminants in Water. *Environ. Sci. Technol.* 46(1), 3655-70.

Cloetens, P., Barrett, R., Baruchel, J., Guigay, J-P., Schlenker, M., 1999. Phase Objects in Synchrotron Radiation Hard X-Ray Imaging. *Journal of Physics D: Applied Physics* 29(1), 133–46. doi:10.1088/0022-3727/29/1/023.

Davis, S.N., Thompson, G.M., Bentley, H.W., Stiles, G., 1980. Ground-Water Tracers — A Short Review. *Groundwater* 18(1), 14–23. doi:10.1111/j.1745-6584.1980.tb03366.x.

Derjaguin, B., Landau, L., 1993. Theory of the Stability of Strongly Charged Lyophobic Sols and of the Adhesion of Strongly Charged Particles in Solutions of Electrolytes. *Progress in Surface Science* 43(1–4), 30–59. doi:10.1016/0079-6816(93)90013-L.

Dominguez, C.M., Rodriguez, S., Lorenzo, D., Romero, A., Santos, A., 2016. Degradation of Hexachlorocyclohexanes (HCHs) by Stable Zero Valent Iron (ZVI) Microparticles. *Water, Air, and Soil Pollution* 227(12), 445-57. doi:10.1007/s11270-016-3149-8.

Dong, H., Blunt, J., 2009. Pore-Network Extraction from Micro-Computerized-Tomography Images. *Physical Review E* 80(3), 1-11. doi:10.1103/PhysRevE.80.036307.

Durenkamp, M., Pawlett, M., Ritz, K., Harris, J.A., Neal, A.L., McGrath, S.P., 2016. Nanoparticles within WWTP Sludges Have Minimal Impact on Leachate Quality and Soil Microbial Community Structure and Function. *Environmental Pollution* 211(1), 399–405. doi:10.1016/j.envpol.2015.12.063.

Elliott, D.W., Zhang, W-X., 2001. Field Assessment of Nanoscale Bimetallic Particles for Groundwater Treatment *Environ. Sci. Technol.* 35(24), 4922–26.

Fagan, P.J., Chase, B., Calabrese, J.C., Dixon, D.A., Harlow, R., Krusic, P.J., Matsuzawa, N., Tebbe, F.N., Thorn, D.L., Wasserman, E., 1992. Some Well Characterized Chemical Reactivities of Buckminsterfullerene (C60). *Carbon* 30(8), 1213–26. doi:10.1016/0008-6223(92)90063-3.

Fedorova, G., Golovko, O., Randak, T., Grabic, R., 2014. Storage Effect on the Analysis of Pharmaceuticals and Personal Care Products in Wastewater. *Chemosphere* 111(1), 55–60. doi:10.1016/j.chemosphere.2014.02.067.

Gaillard, J.F., Chen, C., Stonedahl, S.H., Lau, B.L.T., Keane, D.T., Packman, A.I., 2007. Imaging of Colloidal Deposits in Granular Porous Media by X-Ray Difference Micro-Tomography. *Geophysical Research Letters* 34(18), 2–6. doi:10.1029/2007GL030514.

Hoek, E.M.V., Agarwal, G.K., 2006. Extended DLVO Interactions between Spherical Particles and Rough Surfaces. *Journal of Colloid and Interface Science* 298(1), 50–58. doi:10.1016/j.jcis.2005.12.031.

Ketcham, R.A., 2005. Computational Methods for Quantitative Analysis of Three-Dimensional Features in Geological Specimens. *Geosphere* 1(1), 32–41. doi:10.1130/GES00001.1.

Kocur, C.M., Chowdhury, A.I., Sakulchaicharoen, N., Boparai, H.K., Weber, K.P., Sharma, P., Krol, M.M., Austrins, L., Peace, C., Sleep, B.E., O'Carroll, D.M., 2014. Characterization of nZVI Mobility in a Field Scale Test. *Environmental Science and Technology* 48(5), 2862–69. doi:10.1021/es4044209.

Krol, M.M., Oleniuk, A.J., Kocur, C.M., Sleep, B.E., Bennett, P., Xiong, Z., O'Carroll, D.M., 2013. A Field-Validated Model for in Situ Transport of Polymer-Stabilized nZVI and Implications for Subsurface Injection. *Environmental Science and Technology* 47(13), 7332–40. doi:10.1021/es3041412.

Kumahor, S.K., de Rooij, G.H., Schlüter, S., Vogel, H.-J., 2015. Water Flow and Solute Transport in Unsaturated Sand—A Comprehensive Experimental Approach. *Vadose Zone Journal* 14(2), 0. doi:10.2136/vzj2014.08.0105.

Kumahor, S.K., Hron, P., Metreveli, G., Schaumann, G.E., Vogel, H.-J., 2015. Transport of Citrate-Coated Silver Nanoparticles in Unsaturated Sand. *Sci. Total Environment*. doi:10.1016/j.scitotenv.2015.03.023.

Lapworth, D.J., Baran, N., Stuart, M.E., Ward, R.S., 2012. Emerging Organic Contaminants in Groundwater: A Review of Sources, Fate and Occurrence. *Environmental Pollution* 163(1), 287–303. doi:10.1016/j.envpol.2011.12.034.

Lecoanet, H.F., Bottero, J.-Y., Wiesner, M.R., 2004. Laboratory Assessment of the Mobility of Nanomaterials in Porous Media. *Environ. Sci. Technol.* 38(19), 5164–69.

Lien, H.L., Zhang, W.X., 2001. Nanoscale Iron Particles for Complete Reduction of Chlorinated Ethenes. *Colloids and Surfaces A: Physicochemical and Engineering Aspects* 191(1–2), 97–

105. doi:10.1016/S0927-7757(01)00767-1.

Liu, Y., Blowes, D.W., Groza, L., Sabourin, M.J., Ptacek, C.J., 2014. Acesulfame-K and
Pharmaceuticals as Co-Tracers of Municipal Wastewater in a Receiving River. *Environ. Sci.: Processes Impacts* 16(12), 2789–95. doi:10.1039/C4EM00237G.

Loveland, J.P., Bhattacharjee, S., Ryan, J.N., Elimelech, M., 2003. Colloid Transport in a
Geochemically Heterogeneous Porous Medium: Aquifer Tank Experiment and Modeling. *J. Contam. Hydrol.* 65(3–4), 161–82. doi:10.1016/S0169-7722(02)00238-3.

Machado, S., Stawiński, W., Slonina, P., Pinto, A.R., Grosso, J.P., Nouws, H.P.A., Albergaria,
J.T., Delerue-Matos, C., 2013. Application of Green Zero-Valent Iron Nanoparticles to the
Remediation of Soils Contaminated with Ibuprofen. *Sci. Total Environment* 461–462(1),
323–29. doi:10.1016/j.scitotenv.2013.05.016.

Molnar, I.L., Sanematsu, P.C., Gerhard, J.I., Willson, C.S., O'Carroll, D.M., 2016. Quantified
Pore-Scale Nanoparticle Transport in Porous Media and the Implications for Colloid
Filtration Theory. *Langmuir* 32(31), 7841–53. doi:10.1021/acs.langmuir.6b01233.

Molnar, I.L., Willson, C.S., O'Carroll, D.M., Rivers, M.L., Gerhard, J.I, 2014. Method for
Obtaining Silver Nanoparticle Concentrations within a Porous Medium via Synchrotron X-
Ray Computed Microtomography. *Environ. Sci. Technol.* 48(1), 1114–22.
doi:10.1021/es403381s.

Mompelat, S., Jaffrezic, A., Jardé, E., LeBot, B., 2013. Storage of Natural Water Samples and
Preservation Techniques for Pharmaceutical Quantification. *Talanta* 109(1), 31–45.
doi:10.1016/j.talanta.2013.01.042.

Nowack, B., Bucheli, T.D., 2007. Occurrence, Behavior and Effects of Nanoparticles in the

Environment. *Environmental Pollution* 150(1), 5–22. doi:10.1016/j.envpol.2007.06.006.

O'Carroll, D., Sleep, B.E., Krol, M., Boparai, H., Kocur, C., 2013. Nanoscale Zero Valent Iron

and Bimetallic Particles for Contaminated Site Remediation. *Advances in Water Resources*

51(1), 104–22. doi:10.1016/j.advwatres.2012.02.005.

Patil, S.S., Shedbalkar, U.U., Truskewycz, A., Chopade, B., Ball, A.S., 2015. Nanoparticles for

Environmental Clean-up: A Review of Potential Risks and Emerging Solutions.

Environmental Technology & Innovation 5(1), 10–21. doi:10.1016/j.eti.2015.11.001.

Phenrat, T., Cihan, A., Kim, H.-J., Mital, M., Illangasekare, T., Lowry, G.V., 2010. Transport

and Deposition of Polymer-Modified Fe0 Nanoparticles in 2-D Heterogeneous Porous

Media: Effects of Particle Concentration, Fe0 Content, and Coatings. *Environ. Sci. Technol.*

44(23), 9086–93. doi:10.1021/es102398e.

Praetorrius, A., Tufenkji, N., Goss, K.-U., Scheringer, M., von der Kammer, F., Elimelech, M.,

2014. The Road to Nowhere: Equilibrium Partition Coefficients for Nanoparticles. *Environ.

Sci.: Nano.* 1, 317-323. doi: 10.1039/c4en00043a

Prosen, H., Zupančič-Kralj, L., 2005. Evaluation of Photolysis and Hydrolysis of Atrazine and its

First Degradation Products in the Presence of Humic Acids. *Environmental Pollution*

133(1), 517-529.

Qu, X., Alvarez, P.J.J., Li, Q., 2013. Applications of Nanotechnology in Water and Wastewater

Treatment. *Water Research* 47(12), 3931–46. doi:10.1016/j.watres.2012.09.058.

Reynolds, G W., Hoff, J T., Gillham, R W., 1990. Sampling Bias Caused by Materials Used to Monitor Halocarbons in Groundwater. *Environ. Sci. Technol.* 24(1), 135. doi:10.1021/es00071a017.

Ridler, T.W., Calvard, S., 1978. Picture Thresholding Using an Iterative Slection Method. *IEEE Transactions on Systems, Man and Cybernetics* 8(8), 630–32. doi:10.1109/TSMC.1978.4310039.

Sang, Z., Jiang, Y., Tsoi, Y.K., Leung, K.S.Y., 2014. Evaluating the Environmental Impact of Artificial Sweeteners: A Study of Their Distributions, Photodegradation and Toxicities. *Water Research* 52(1), 260–64. doi:10.1016/j.watres.2013.11.002.

Sasidharan, S., Torkzaban, S., Bradford, S., Dillon, P.J., Cook, P.G., 2014. Coupled Effects of Hydrodynamic and Solution Chemistry on Long-Term Nanoparticle Transport and Deposition in Saturated Porous Media. *Colloids and Surfaces A: Physicochemical and Engineering Aspects* 457(1), 169–79. doi:10.1016/j.colsurfa.2014.05.075.

Schneider, C., Rasband, W.S., and Eliceiri, K.W., 2012. NIH Image to ImageJ: 25 Years of Image Analysis. *Nature Methods* 9(7), 671–75. doi:10.1038/nmeth.2089.

Son, H.A., Yoon, K.Y., Lee, G.J., Cho, J.W., Choi, S.K., Kim, J.W., Im, K.C., Kim, H.T., Lee, K.S., Sung, W.M., 2015. The Potential Applications in Oil Recovery with Silica Nanoparticle and Polyvinyl Alcohol Stabilized Emulsion. *Journal of Petroleum Science and Engineering* 126(1), 152–61. doi:10.1016/j.petrol.2014.11.001.

Spanne, P., Rivers, M.L., 1987. Computerized Microtomogaphy Using Synchrotron Radiation from the NSLS. *Nuclear Instruments and Methods in Physics Research* 25(1), 1063–67.

Stimson, J., Chae, G.-t., Ptacek, C.J., Emelko, M.B., Mesquita, M.M., Hirata, R.A., Blowes, D.W., 2010. Basic Oxygen Furnace Slag as a Treatment Material for Pathogens : Contribution of Inactivation and Attachment in Virus Attenuation. *Water Research* 44(4), 1150–57. doi:10.1016/j.watres.2009.11.054.

Su, C., Puls, R.W., Krug, T., Watling, M.T., O'Hara, S.K., Quinn, J.W., Ruiz, N.E., 2012. A Two and Half-Year-Performance Evaluation of a Field Test on Treatment of Source Zone Tetrachloroethene and Its Chlorinated Daughter Products Using Emulsified Zero Valent Iron Nanoparticles. *Water Research* 46(16), 5071–84. doi:10.1016/j.watres.2012.06.051.

Tessier, A., Fortin, D., Belzile, N., DeVitre, R. R., Leppard, G. G., 1996. Metal Sorption to Diagenetic Iron and Manganese Oxyhydroxides and Associated Organic Matter: Narrowing the Gap between Field and Laboratory Measurements. *Geochimica et Cosmochimica Acta* 60(3), 387–404. doi:10.1016/0016-7037(95)00413-0.

Tomizawa, M., Kurosu, S., Kobayashi, M., Kawase, Y., 2016. Zero-Valent Iron Treatment of Dark Brown Colored Coffee Effluent: Contributions of a Core-Shell Structure to Pollutant Removals. *Journal of Environmental Management* 183(1), 478–87. doi:10.1016/j.jenvman.2016.08.081.

Toride, N., Leij, F J., van Genuchten, M Th., 1995. The CXTFIT Code for Estimating Transport Parameters from Laboratory or Field.

Tosco, T., Bosch, J., Meckenstock, R.U., Sethi, R., 2012. Transport of Ferrihydrite Nanoparticles in Saturated Porous Media: Role of Ionic Strength and Flow Rate. *Environmental Science and Technology* 46(7), 4008–15. doi:10.1021/es202643c.

Tratnyek, P.G., Johnson, R.L., 2006. Nanotechnologies for Environmental Clean Up. *Nanotoday* 1(2), 44–48.

U.S. EPA., 2010. Stability of Pharmaceuticals, Personal Care Products, Steroids, and Hormones in Aqueous Samples, POTW Effluents, and Biosolids, no. September.

Van Stempvoort, D.R., Roy, J.W., Brown, S.J., Bickerton, G., 2011. Artificial Sweeteners as Potential Tracers in Groundwater in Urban Environments. *Journal of Hydrology* 401(1–2), 126–33. doi:10.1016/j.jhydrol.2011.02.013.

VandeVoort A.R., Arai, Y., 2012. Effect of Silver Nanoparticles on Soil Denitrification Kinetics. *Industrial Biotechnology*, 358–65. doi:10.1089/ind.2012.0026.

Verwey, E J W., 1947. Theory of the Stability of Lyophobic Colloids. *The Journal of Physical and Colloid Chemistry* 51(3), 631–36. doi:10.1038/162315b0.

Wong, M.S., Alvarez, P.J.J., Fang, Y.-l., Nutt, M.O., Miller, T., Heck, K.N., 2009. Cleaner Water Using Bimetallic Nanoparticle Catalysts. *J. Chem. Technol. Biotechnol.* 84(1), 158–66. doi:10.1002/jctb.2002.

Yao, K.-m., Habibian, M.T., O'Melia, C.R., 1971. Water and Waste Water Filtration: Concepts and Applications. *Environ. Sci. Technol.* 5(11), 1105–12. doi:10.1021/es60058a005.

Zhan, J., Sunkara, B., Le, L., John, V.T., He, J., McPherson, G.L., Piringer, G., Lu, Y., 2009. Multifunctional Colloidal Particles for in Situ Remediation of Chlorinated Hydrocarbons *Environ. Sci. Technol.* 43(22), 8616–21.

Zhang, W.-x., 2003. Nanoscale Iron Particles for Environmental Remediation : An Overview.

Journal of Nanoparticle Research 5(1), 323–32.

Appendix A:

ImageJ Macro for Data Processing

```
//-----------------------------------------------------------------------------------------//
//   Tomography Image Processing Macro: Ottawa Sand                    //
//   E. Saurette, July 2015                                           //
//   Thanks to Dr. T. Al's 'Difference Image Macro 30_10_14' for guidance    //
//   Extra special thanks to Wayne Rasband and Curtis T Rueden         //
//    for their time and help through the ImageJ email list           //
//-----------------------------------------------------------------------------------------//
  Dialog.create("WELCOME USER");
//
// Welcome to the Tomography Image Processing Macro. This macro will take two directories of
images (reconstructed and difference images) and process them to give aqueous and porous
media segmented images, aqueous and porous media segmented images with difference image
gray scale values, and a csv .txt file with the average gsv for each slice of each segmented image
as well as the porosity of each slice. Are you ready to begin?|
//
  Dialog.show();
//
// Setting up the directories which will be used in the macro.
//
  dir1 = getDirectory("Choose the Directory for Above K-Edge Recon Volume Files");
  dir2 = getDirectory("Choose the Directory for Difference Volume Files");
  dir3 = getDirectory("Choose the Directory for Silica Grains Segmented");
  dir4 = getDirectory("Choose the Directory for Aqueous Phase Segmented");
  dir5 = getDirectory("Choose the directory for Silica Grains Final");
  dir6 = getDirectory("Choose the Directory for Aqueous Phase Final");
  dir7 = getDirectory("Choose the Master Directory");
//
// Setting up the input parameters that we will use for cropping and also for exporting the data
//
  Dialog.create("SET UP INPUT PARAMETERS");
//
  Dialog.addMessage("RECTANGULAR ROI FOR CROPPING");
  Dialog.addNumber("X Value; 0 for no cropping:", 720);
  Dialog.addNumber("Y Value; 0 for no cropping:", 720);
  Dialog.addNumber("Width; total Width for no cropping:", 720);
  Dialog.addNumber("Height; total Height for no cropping:", 720);
//
  Dialog.addMessage("PROVIDE A NAME FOR THE OUTPUT TEXT FILE");
  fname = "Col_LETTER";
  Dialog.addString("File Name:", fname);
  Dialog.show();
//
// Saving the cropping parameters and file name as variables
//
  RECTX = Dialog.getNumber();
  RECTY = Dialog.getNumber();
```

```
  RECTW = Dialog.getNumber();
  RECTH = Dialog.getNumber();
  fname = Dialog.getString();
  f = File.open(dir7+fname+".txt");
//
// Set up the header in the log for generating 1-D profiles
//
  print("Average gray scale values are listed below for each slice");
  print(" ");
  print("Rectangle ROI coordinates for cropping: "+"X = "+RECTX+"; Y = "+RECTY+"; W =
"+RECTW+"; H = "+RECTH);
  print(" ");
  print("Image Title, "+"Slice Number, "+"Average GSV");
//
// Set up the header in the output file for generating 1-D profiles
//
  print(f, "Average gray scale values are listed below for each slice");
  print(f, " ");
  print(f,"Rectangle ROI coordinates for cropping: "+"X = "+RECTX+"; Y = "+RECTY+"; W =
"+RECTW+"; H = "+RECTH);
  print(f, " ");
  print(f,"Image Title, "+"Slice Number, "+"Average GSV");
//
  setBatchMode(false);  // prevents display of images when set to TRUE - set to false only for
debugging (or if you want to watch!)
//
// Getting the file names that are in the Recon and Diff directories and saving them as an array
//
  list1 = getFileList(dir1);
  list2 = getFileList(dir2);
//
// Starts counting how many images have been processed
//
  count = 0;
//
// Looping through the list of Recon images in order to process them all in sequence
//
  for (i=0; i<list1.length; i++) {
                path1 = dir1+list1[i];
//
// These lines are from the plugin "GSETomo" which open netcdf files (.volume included)
//
                run("Load NetCDF File", "open=[" + path1 +"] single variable");
                showProgress(count++, list1.length);
                run("XOR...", "value=1000000000000000 stack");
                run("Calibrate...", "function=[Straight Line] unit=[Gray Value] text1=[0 65535]
```

text2=[-32768 32767]");

```
                run("Enhance Contrast", "saturated=0.5")
//
// Specifying the ROI and cropping the Recon image to that size
//
                makeRectangle(RECTX, RECTY, RECTW, RECTH);
                run("Crop");
//
// Changing the image from a 16-bit image to an 8-bit image
//
                run("8-bit");
//
// The segmentation technique begins now, including Auto Thresholding, using a median filter
// with rolling ball radius of 2 pixels, and then using erode twice to remove holes.
//
                run("Smooth", "stack");
                run("Median...", "radius=4 stack");
                run("Auto Threshold...", "method=Default white stack");
                run("Dilate", "stack");
                run("Dilate", "stack");
//
// Taking the segmented image, saving it's unique ImageID and also giving it a sequenced output
// name
//
                IDb = getImageID();
                outputname = "PM_"+i;
                rename(outputname);
        saveAs("Tiff", dir3+outputname+".tif");
//
// Duplicated the segmented image in order to give the aqueous segments a non-zero value (255),
// and changing that non-zero value to 1
//
        run("Duplicate...", "title=new.tif duplicate range=1-1200");
    run("Auto Threshold...", "method=Default stack");
        run("Macro...", "code=[if(v==255) v=1] stack");
    IDc = getImageID();
    outputname = "AQ_"+i;
    rename(outputname);
        saveAs("Tiff", dir4+outputname+".tif");
//
        frames=nSlices;
//
// Defining what action the program should run on these slices these can be added or subtracted
// check Set Measurements for possibilities
//
                run("Set Measurements...", " mean min integrated redirect=None decimal=4");
```

```
                run("Clear Results");
//
// Looping over each slice in the AQ_i stack to obtain the mean GSV for each slice, to obtain
porosity
//
                for(n=0; n<frames; n++) {
                        currentslice=n+1;
                        setSlice(currentslice);
                        run("Measure");
                        avggsv=getResult("Mean");
                        print(f,outputname+","+n+","+avggsv);
                }
//
// Opening the difference image in order to multiply it by the segmented images to isolate the
GSVs associated with the PM and the AQ portions of the image
//
                path2 = dir2+list2[i];
//
// These lines are from the plugin "GSETomo" which open netcdf files (.volume included)
//
                run("Load NetCDF File", "open=[" + path2 +"] single variable");
                run("XOR...", "value=1000000000000000 stack");
                run("Calibrate...", "function=[Straight Line] unit=[Gray Value] text1=[0 65535]
text2=[-32768 32767 ]");
                run("Enhance Contrast", "saturated=0.5");
//
                IDe = getImageID();
                run("Set Scale...", "distance=1 known=2.79 pixel=1 unit=um");
                makeRectangle(RECTX, RECTY, RECTW, RECTH);
                run("Crop");
                IDd = getImageID();
                imageCalculator("Multiply create 32 bit stack", IDb, IDd);
                outputname = "PM_FINAL_"+i;
                rename(outputname);
            saveAs("Tiff", dir5+outputname+".tif");
//
        frames=nSlices;
//
// Defining what action the program should run on these slices these can be added or subtracted
check Set Measurements for possibilities
//
                run("Set Measurements...", " mean min integrated redirect=None decimal=4");
                run("Clear Results");
//
// Looping over each slice in the PM_Final stack to obtain the mean GSV for each slice
//
```

```
                for(n=0; n<frames; n++) {
                        currentslice=n+1;
                        setSlice(currentslice);
                        run("Measure");
                        avggsv=getResult("Mean");
                        print(f,outputname+","+n+","+avggsv);
                }
                close();

        imageCalculator("Multiply create 32 bit stack", IDc, IDd);
        outputname = "AQ_FINAL_"+i;
                rename(outputname);
        saveAs("Tiff", dir6+outputname+".tif");
//
        frames=nSlices;
//
// Defining what action the program should run on these slices these can be added or subtracted
check Set Measurements for possibilities
//
                run("Set Measurements...", " mean min integrated redirect=None decimal=4");
                run("Clear Results");
//
// Looping over each slice in the AQ_Final stack to obtain the mean GSV for each slice
//
                for(n=0; n<frames; n++) {
                        currentslice=n+1;
                        setSlice(currentslice);
                        run("Measure");
                        avggsv=getResult("Mean");
                        print(f,outputname+","+n+","+avggsv);
                }
        close();
        selectImage(IDb);
        close();
        selectImage(IDc);
        close();
        selectImage(IDd);
        close();
        run("Clear Results");
        }
print(count+" files processed");
print("All done!");
```